5. MARE MATERIALS

FIGURE 5.1 (OVERLEAF). —Lobate mare-basalt flows in Mare Imbrium. Apollo 15 frame M–1556.

5. MARE MATERIALS

CONTENTS

INTRODUCTION

The darker half of the Galilean dichotomy, the smooth maria, are topographically and geologically simpler than the ringed basins that contain them. The maria are the most earthlike and probably the most easily understood lunar features (fig. 5.1). They cover about 16 percent of the lunar surface, or 30 percent of the nearside and 2 percent of the farside. If younger craters were absent, maria would cover about an additional 1 percent of the Moon (dashed contacts, pl. 4). Most maria flood large basins and their peripheral depressions; they also flood craters and small basins that are superposed on larger basins. Some mare occurrences have led to the identification of basins where none were otherwise suspected. A few small maria that are not related to known basins (pl. 4; figs. 5.2, 5.3) may, similarly, indicate the presence of undiscovered basins.

Because of their resemblance to terrestrial volcanic terranes, the maria were more readily interpreted before being sampled than were the terrae. The approximately level mare surfaces were correctly taken as signs of fluid, lavalike emplacement (Gilbert, 1893; Urey, 1952; Baldwin, 1949, 1963; Kuiper, 1959; Shoemaker and Hackman, 1962). Their landforms were perceived as analogous to volcanic landforms on the Earth (Kuiper, 1959; Shoemaker and Hackman, 1962; Quaide, 1965). Although nonbasaltic composition (especially ash-flow tuff; O'Keefe and Cameron, 1962; Mackin, 1969) and such exotic origins as mobile dust (Gold, 1955) and water-laid sediment (Gilvarry, 1970) were considered, the low albedo and certain diagnostic landforms suggested basic lava to most workers (for example, Baldwin, 1963, p. 336). Basaltic composition seemed to be substantiated by Surveyor 5 and 6 analyses in 1967 (Gault and others, 1968a, p. 287), and was established by the Apollo 11 samples in July 1969. Basalt has been returned from all the mare sites visited. The rock name "basalt" can thus be used as a near-synonym for the less committal term "mare materials," even in unsampled regions.[5.1]

[5.1] Strictly speaking, the term "maria" (singular and adjectival form, "mare") refers to the surfaces, and "mare materials" to the rock-stratigraphic units that underlie the surfaces; however, "mare" and "maria" are commonly used for the materials as well.

Stratigraphic relations of the mare-basalt flows are also readily understood in principle because they are similar to relations familiar on the Earth. The margins of the flows follow the contours of the containing basins, as would any later fluidlike deposits. Relative crater densities are consistent with the younger age of these flows.

FIGURE 5.2.—Isolated mare patch in crater Kohlschütter (arrow; 53 km, 27° N., 154° E.). Many craters of subequal size are probably secondary to Mendeleev basin (see chap. 9), outside lower left corner of scene. Boom of Apollo 16 gamma-ray spectrometer protrudes into view at right. Apollo 16 frame M–729.

The main obstacle to acceptance of these obvious relations was the peculiar confusion between mare and basin (see chap. 2), which persisted until the early 1960's and is still not entirely dispelled.

By definition, mare materials (1) form generally smooth and level surfaces and (2) are dark. In some areas, mare units can be subdivided by their topographic characteristics. However, most subdivisions are based on optical, spectral, or geochemical properties commonly called remote-sensing properties. In this respect, mare units differ from impact units, because they are igneous-rock bodies whose compositional unity is more obvious than is morphology due to emplacement. The recognition of mare subunits has advanced greatly since 1972 over its rather primitive status before Apollo exploration (Head and others, 1978b). The following sections discuss the properties by which maria and their subunits are recognized and interpreted by remote observations, and the last section of this chapter briefly describes and interprets the samples of mare basalt returned from the Moon.

MAPPING PROPERTIES

Morphology

Certain areally minor, though genetically significant, morphologies interrupt the flat mare surfaces. The most significant are *lava-flow fronts*. These lobate edges resemble terrestrial lava lobes and thus indicate that at least some maria consist of volcanic lavas. The first flow fronts to be described and the largest yet known are in Mare Imbrium (fig. 5.1; Schaber, 1969). They are visible in good telescopic photographs and were shown to coincide with color boundaries, presumed to be some sort of compositional contacts (Kuiper, 1965, p. 29–32; Whitaker, 1966, p. 79–83). These observations quieted exotic hypotheses of mare origin in the minds of most workers. The Imbrium lobes range from 10 to more than 35 m in height and bound flows as much as 1,200 km long (Schaber, 1973). These great dimensions may indicate that each flow formed by rapid eruption of fluid lava from a single large vent (Schaber, 1973). The Imbrium flows are probably the only relatively recent large flows still exposed, although earlier, now-buried eruptions may have been equally large. Scarps of shorter and thinner flows are observed in Oceanus Procellarum, Mare Cognitum, Mare Vaporum, and Sinus Medii (Schaber and others, 1976).

Otherwise, lunar mare flows are either too thin or, alternatively, too floodlike (Holcomb, 1971; Greeley, 1976) to have formed lobate scarps. A pooled, massive style of some mare units is suggested by marginal terraces (fig. 5.3). Holcomb (1971) pointed out the similarity of these "bathtub rings" perched on the terrae around some maria to those left by subsidence of Hawaiian lava lakes. The terraces suggest withdrawal of ponded lava by way of observed sinuous rilles (fig. 5.4; Holcomb, 1971; K.A. Howard, in Carr and others, 1971; Howard and others, 1972; Greeley and Spudis, 1978).

Several types of positive landforms, mostly formed by extrusion of basalt, are scattered in several, and concentrated in a few, maria (pl. 4; Guest and Murray, 1976). Most *domes* are subtle circular features with low profiles, commonly topped by small smooth-rimmed craters (figs. 5.5, 5.6); they are visible in telescopic visual observations or photographs made at low Sun illuminations (Arthur, 1962). The apparent internal origin of the domes was a major factor in endogenic interpretations of the maria, and their low profiles suggested fluid volcanism characteristic of mafic magmas. Low mare domes are concentrated in Mare Tranquillitatis (Vitruvius region, fig. 5.5) and western Mare Insularum (Hortensius and Milichius regions, fig. 5.6) but occur in other maria as well. Steeper, rough-surfaced features commonly called *cones* are concentrated in the Marius Hills (fig. 5.7; McCauley, 1967a, b, 1968, 1969b; Guest, 1971) and are scattered in several maria, for example, Mare Cognitum, Mare Tranquillitatis (Wilhelms, 1972a), and the border of Mare Serenitatis (Bryan and Adams, 1973; Scott, 1973). Some cones occur in the terrae (fig. 5.8). The difference between the domes and cones presumably reflects variations in composition or in the eruptive process, and the Marius Hills were a favored site for Apollo missions in hopes that they would yield differentiated volcanic-rock types (McCauley, 1969b). The morphologies of domes or cones are mimicked by *kipukas* or *steptoes*, synonyms for protruding terra or mare deposits isolated from the rest of their geologic unit by floods of later mare materials (see fig. 6.3). The Rümker hills (fig. 5.9) apparently consist of several domes and other mare-related units partly burying Imbrium-radial terra (Guest, 1971). None of the positive lunar volcanic landforms remotely approaches a terrestrial or martian shield volcano or stratovolcano in size. Almost all the landforms listed here occur in shallow maria (Arthur, 1962, p. 322; Head, 1976a). Some 200 such landforms were recently classified by Head and Gifford (1980).

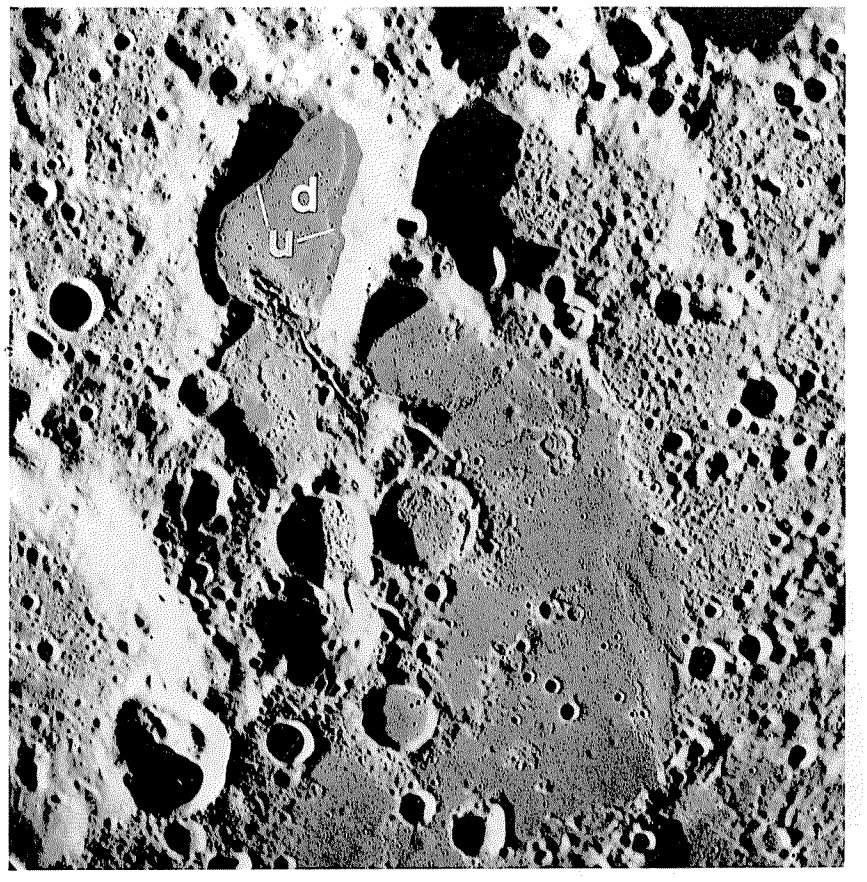

FIGURE 5.3.—Lacus Solitudinis, showing down (d) and up (u) sides of marginal terraces of mare. Scene centered at 27° S., 103° E. Apollo 15 frame M–2627.

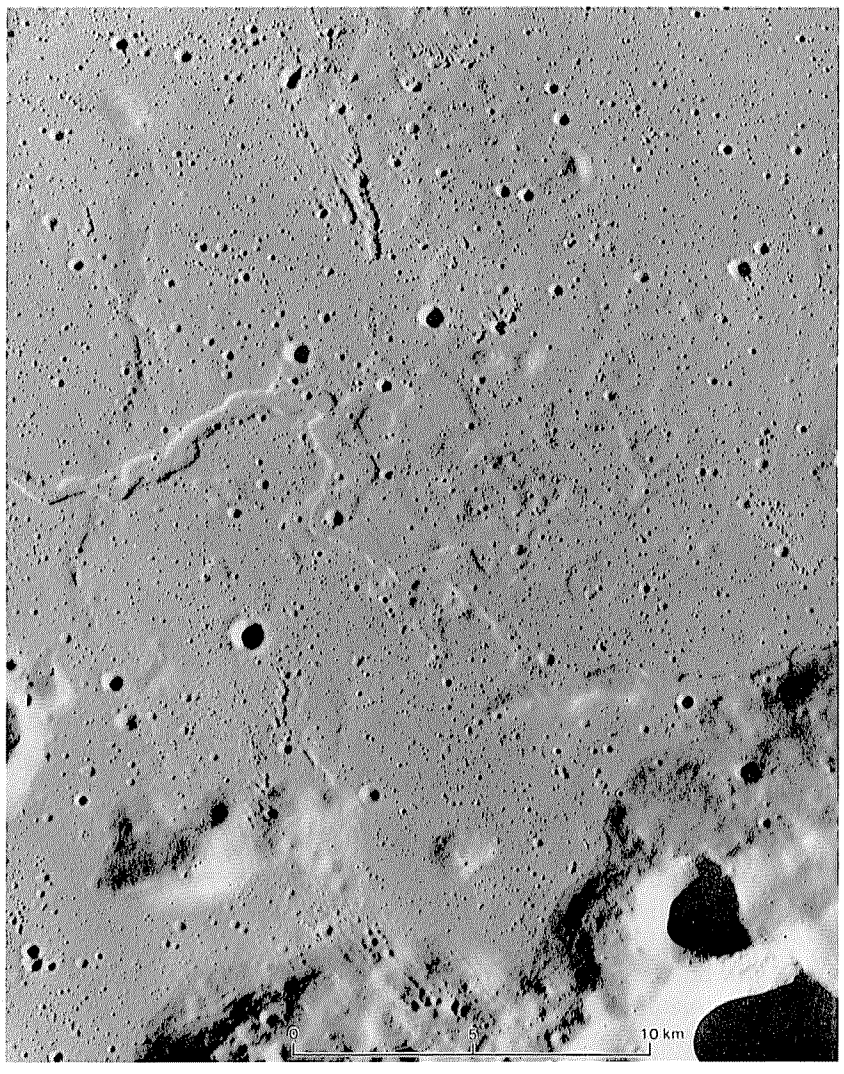

FIGURE 5.4.—"Scablands" north of Aristarchus Plateau. Mare lava probably drained out of the region in the sinuous rille (left). Large craters in lower right are possibly secondary to Orientale basin. Scene centered at 30° N., 53.5° W. Apollo 15 frame P–349.

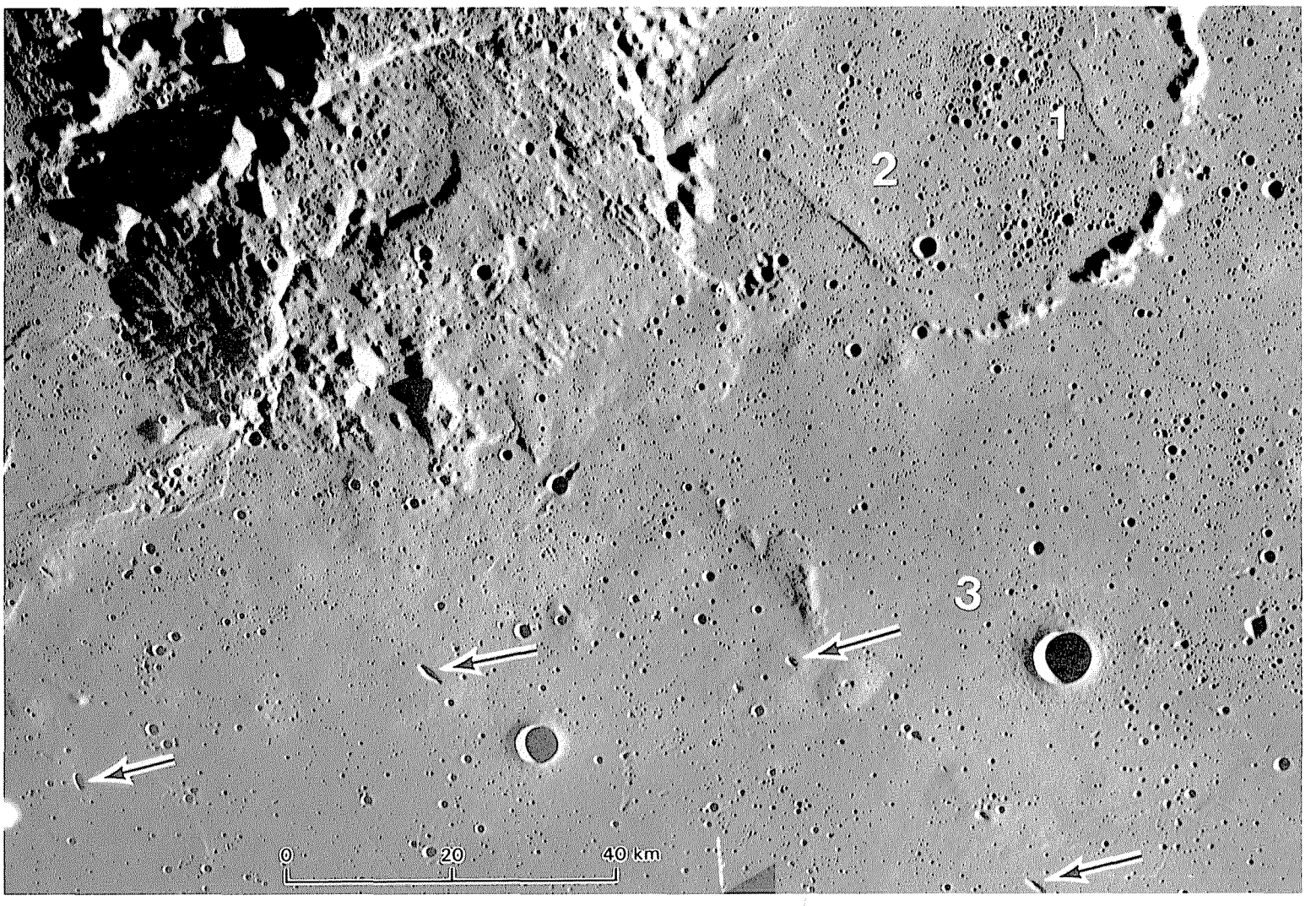

FIGURE 5.5.—Mare domes in northern Mare Tranquillitatis. Numerous elongate pits are on summits of low domes or in flat mare (arrows). Mare units are numbered in order of decreasing age. Crater below number 3 (youngest unit) is Maraldi B (7 km). Scene centered at 15° N., 35° E. Apollo 17 frame M–305.

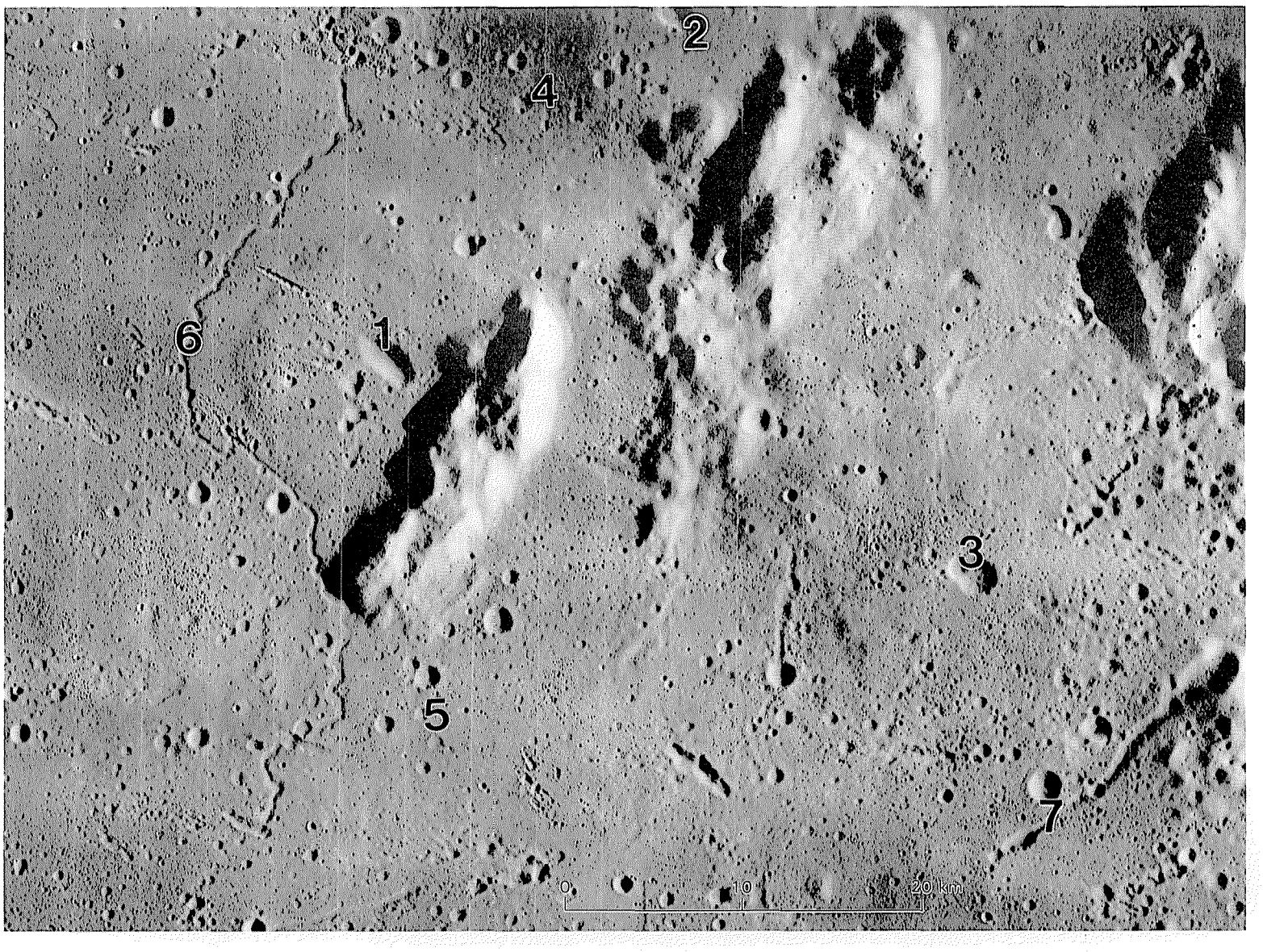

FIGURE 5.6.—Detail of mare domes and other endogenic features, including circular domes with elongate central craters (1, 2); irregular domes with circular, nevertheless probably endogenic, craters (3); concentrations of similar large, soft-appearing circular craters that could be endogenic (4, 5); sinuous rille (6); and elongate endogenic vent or collapse feature (7). Scene centered at 13° N., 30.5° W. Orbiter 5 frame M–164.

Visible source vents are rare in the maria, because the lavas probably cover their sources as do flood-basalt lavas on the Earth (Greeley, 1976). Some *endogenic craters* do appear amidst the maria, however, and are fairly numerous along their borders (figs. 5.10*A–D*); others lie in small patches of dark material in the terrae (figs. 5.8, 5.10*E–H*). Their internal origin is determined by this association with volcanic materials or by their alignment along faults. For example, random impact is unlikely to be responsible for the many craters exactly centered on what are evidently volcanic domes (figs. 5.5, 5.6). The craters or rimless pits along Rima Hyginus are similarly eliminated statistically as impact craters because they are perfectly aligned along the rille (fig. 5.10*E*). Although one leg of Rima Hyginus is radial to the Imbrium basin, both the rilles and the craters are too young to have been formed directly by the impact (see chap. 6; Wilhelms, 1968; Pike, 1976). Like many other endogenic craters (figs. 5.10*A–D*), the rille craters and the main Hyginus crater at the rille "elbow" could have formed entirely by collapse without the extrusion of any material (Pike, 1976). Single craters situated along rilles, amidst dark materials, and with elongate or irregular shapes are also probably endogenic (figs. 5.10*F–H*). A few craters not situated along rilles resemble secondary-impact craters, but endogeny may be assumed if the craters are highly irregular and are centered in dark deposits (figs. 5.10*G, H*). Although the dark ejecta of endogenic craters is commonly more extensive relative to the crater size than is the ejecta of impact craters (table 3.1), the volcanic ejecta is smoother, and the craters are all small (mostly less than 10 km diam). Despite the early popularity of a caldera origin for such large craters as the smooth-rimmed class (fig. 3.15), large calderas are not expected on the Moon; calderas form by collapse or magma withdrawal into shallow magma chambers, which probably never existed on the Moon.

Sinuous rilles are another areally minor but visually arresting type of mare feature. The Apollo 15 landing was targeted next to a large sinuous rille, Rima Hadley (fig. 5.11; chaps. 10, 11). Several other rilles were considered for landings to determine their formational

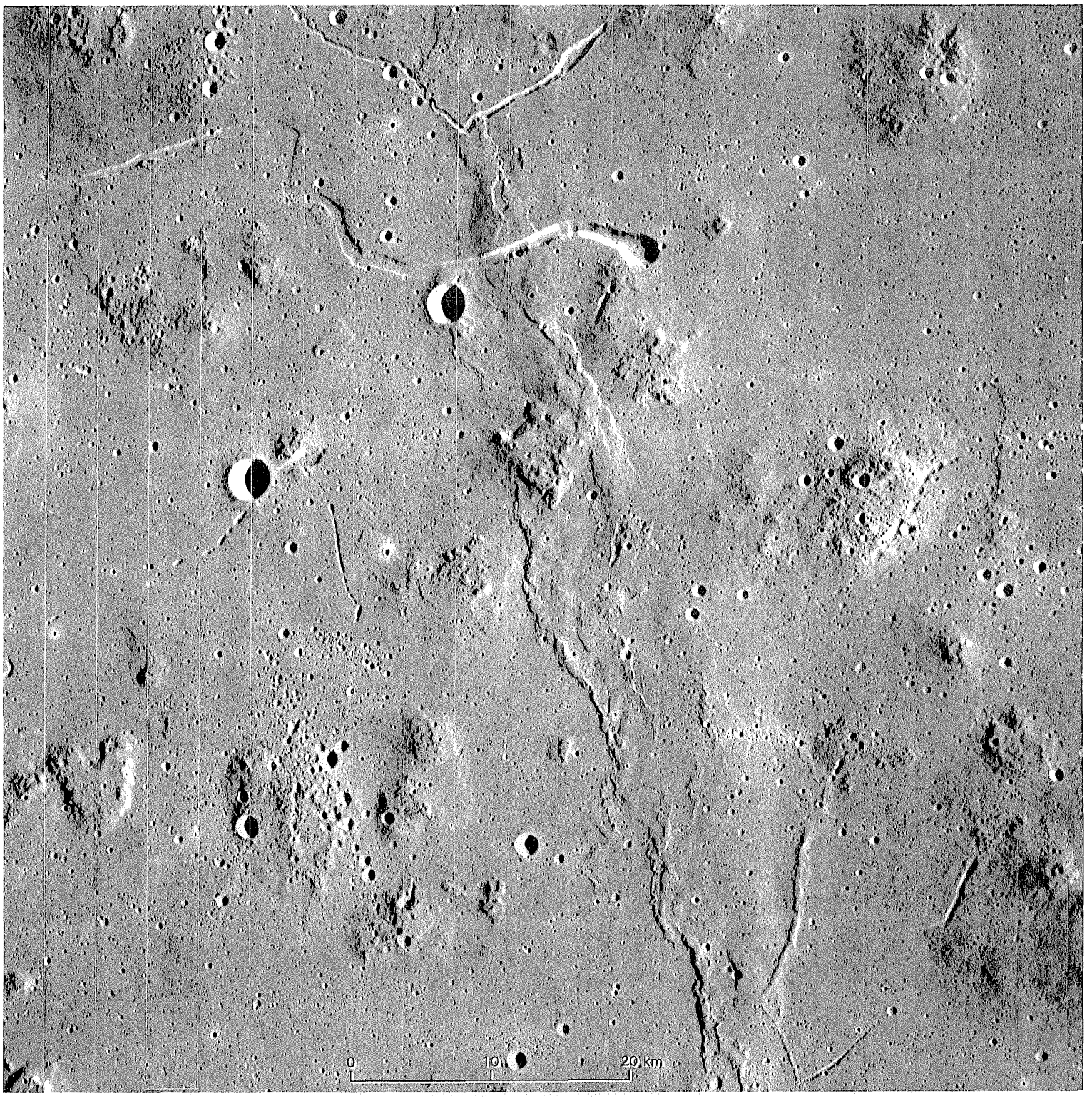

FIGURE 5.7.—Marius Hills, a complex of diverse, rough-textured domes or cones surrounded by smoother mare materials. Orbiter 5 frame M–211.

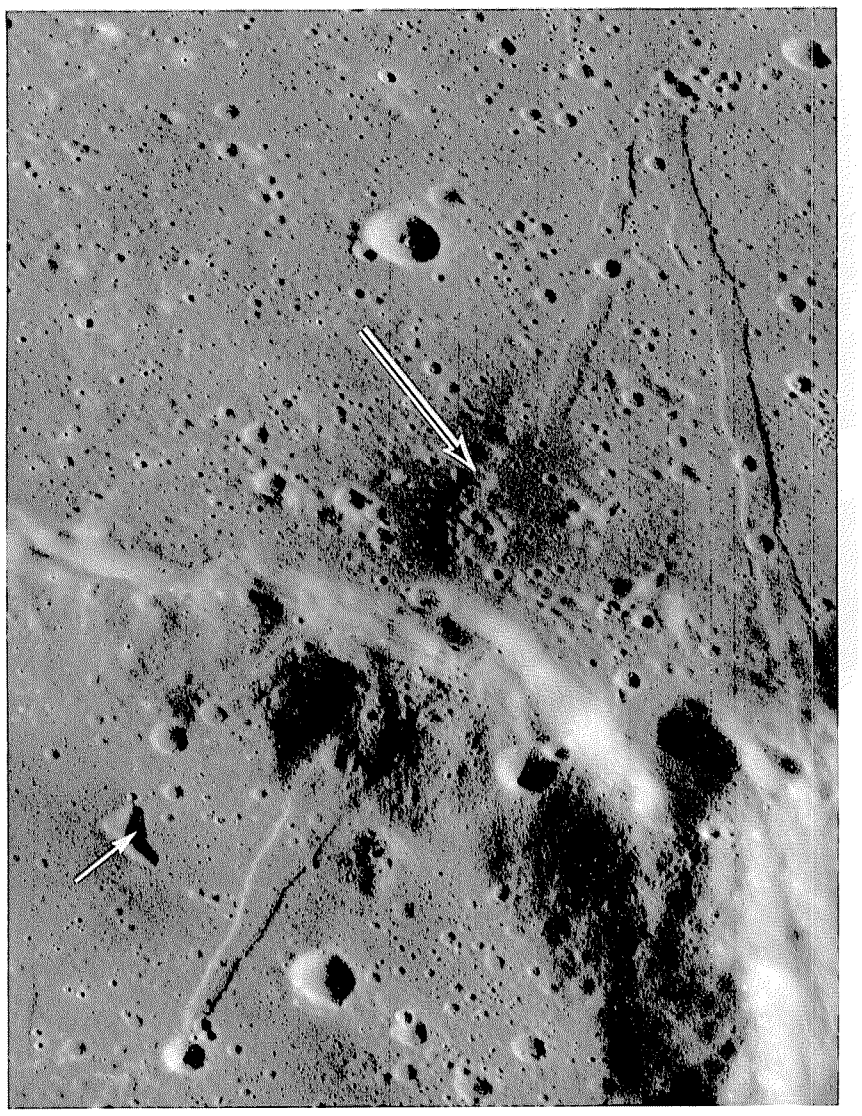

FIGURE 5.8.—Rough cones (black-and-white arrow) situated along linear rille and amidst dark-mantling material or mare lava. Smooth-profiled irregular pit (white arrow) further indicates basaltic volcanism in this terra setting. Crater rim separates craters Fra Mauro (above) and Bonpland (below). Black-and-white arrow is 5 km long; scale varies because of obliquity. Apollo 16 frame P–5425.

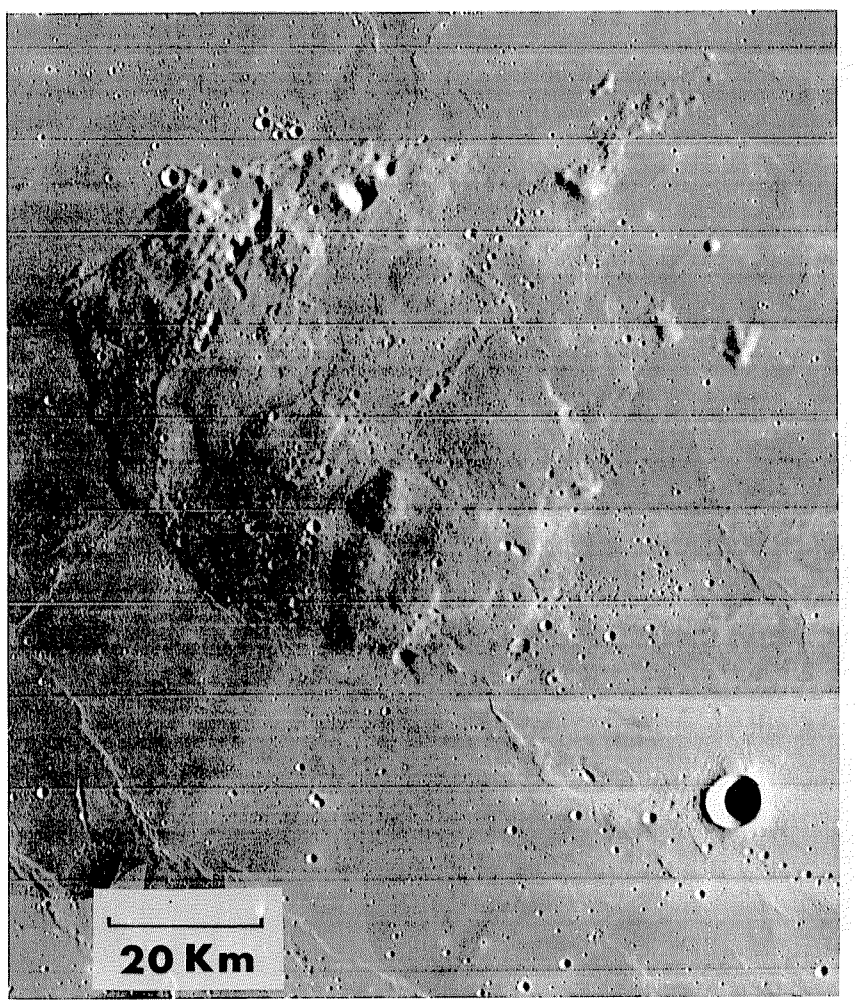

FIGURE 5.9.—Rümker hills (Mons Rümker), a complex of subdued hills in northern Oceanus Procellarum (41° N., 58° W.). Imbrium-radial lineations (upper right to lower left) suggest an origin as terra covered by thin layer of dark-mantling material.

process and to collect samples of volatile or other exotic erupted materials (fig. 5.12). Fieldwork on the Earth and at Rima Hadley has shown that these meandering grooves are probably lava channels or collapsed lava tubes, which are the sites of the last flows of molten magma in a lava unit (Kuiper and others, 1966, p. 199; Oberbeck and others, 1969; Greeley, 1971; Murray, 1971; Cruikshank and Wood, 1972; Howard and others, 1972; Guest and Greeley, 1977, p. 62–68). Very long and narrow rilles are likely to have been channels (always open); others, including Hadley, display alternately roofed and unroofed segments that indicate an origin as tubes (figs. 5.11, 5.13). The sources of some lunar rilles are in the terra or at the mare-terra contact (figs. 5.11, 5.12). Several appear to have erosionally incised the substrate, including terra material (fig. 5.12*C*; Carr, 1974). Sinuous rilles and other volcanic landforms of the maria were thoroughly described and illustrated by Lowman (1969), Schultz (1976b), and Masursky and others (1978).

Blanketing

The property of blanketing or mantling terra topography distinguishes another class of dark, mare-related units, the *dark-mantling materials*. They are as dark as or darker than the maria, but their observed relief is partly rugged. The largest and most numerous tracts with this seemingly anomalous combination of properties lie around the southern periphery of the Imbrium basin (pl. 4; figs. 1.6, 1.7, 5.14, 5.15). This position led to their interpretation as a dark facies of Imbrium ejecta (Shoemaker and Hackman, 1962; Hackman, 1966). Carr (1965a, 1966a, b), however, showed that the large dark areas on the southeast slope of Montes Apenninus are not composed of Imbrium ejecta. He observed that flat surfaces next to the dark ejecta are equally dark, and so the same dark material probably covers both the ejecta and the much younger mare material (fig. 5.16). Moreover, other patches of mantling material are peripheral to Mare Serenitatis (figs. 5.17, 5.18; Carr, 1965a, 1966a, b), Mare Humorum (Titley, 1967), Mare Nectaris (Elston, 1972), Mare Crisium (Olson and Wilhelms, 1974), Mare Smythii (Wilhelms and El-Baz, 1977), Oceanus Procellarum (Moore, 1965, 1967; McCauley, 1967a, b), and, in fact, all carefully scrutinized maria (pl. 4; Head, 1974a, 1976a; Wilhelms, 1980). This concentration near maria and the dark color indicate a genetic relation of the dark-mantling materials to the maria. The flat parts of maria may also contain dark-mantling materials, but these are difficult to distinguish from mare lavas.

A more specific origin for the dark-mantling materials is suggested by other physical properties. On both telescopic and spacecraft photographs, they appear fine-textured, relatively uncratered, and smoother than the underlying topography (figs. 5.15, 5.16). No blocks are visible in the 2-m resolution of the best Apollo photographs. Mantles drape differentially over mountains, low hills, and flat surfaces, and are thickest in depressions and thin or absent on sharp hills. The brightness of some hilltops surrounded by the deposits indicates nondeposition or shedding of the dark material. Shedding is the preferred explanation because some dark deposits lie at higher elevations than some bright summits. Also, the action of mass wasting is indicated by talus streaks that descend from the bright outcrops (fig. 5.16). Shedding is consistent with the propensity of unconsolidated material to slide downslope.

The morphologic properties and distribution of the dark-mantling materials suggest that they consist of volcanic fragments, *pyroclastic* material. The Marius Hills (McCauley, 1964a), the Aristarchus Plateau, and Montes Harbinger (figs. 5.7, 5.12*A*; Moore, 1964b) were originally interpreted as terra features covered by volcanic ash (figs. 5.7, 5.12). Carr (1965a, 1966a, b) noted that the dark deposits are situated near likely eruptive fissures in the form of rilles in the maria (fig. 5.16). Unlike lavas, few dark-mantling materials lack elongate or irregular, commonly rille-straddling craters, gashes, or dark cones that are likely source vents (figs. 5.8, 5.10*F–H*, 5.12, 5.16). Pyroclastic origin was favored for the dark-mantling materials in all the early photogeologic work and has been confirmed by sampling data (see chap. 11). The dark halos of many small endogenic craters, such as those in Alphonsus (fig. 5.10*F*), are also dark-mantling deposits. Head and Wilson (1979), however, suggested that the eruptive mechanisms differ: The extensive, regional deposits are thought to be strombolian (continuous eruptions), and the smaller halos vulcanian (intermittent eruptions).

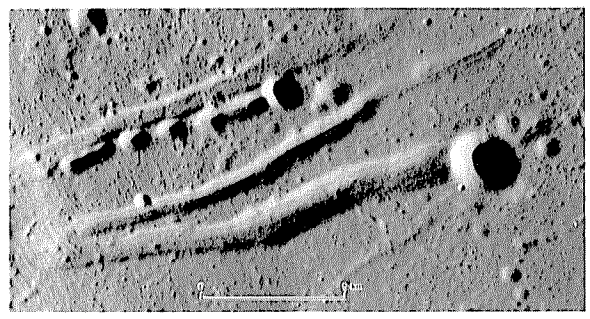

A

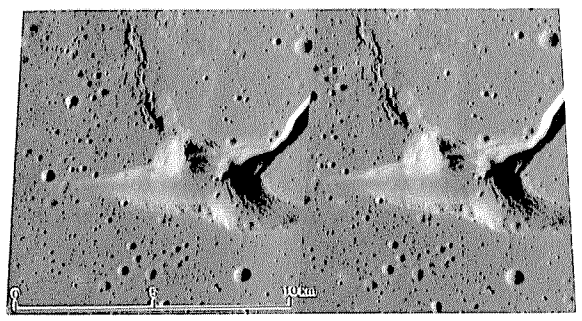

B

C

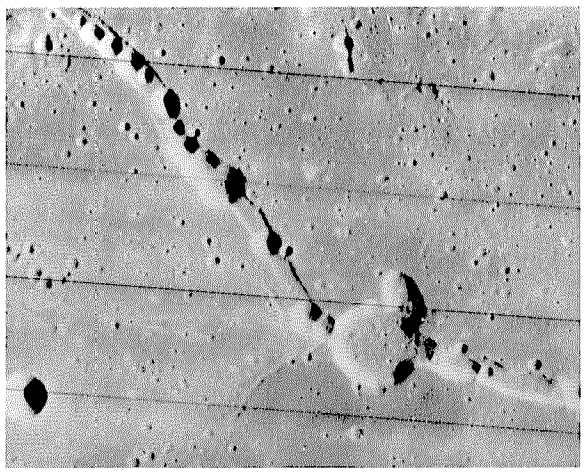

E

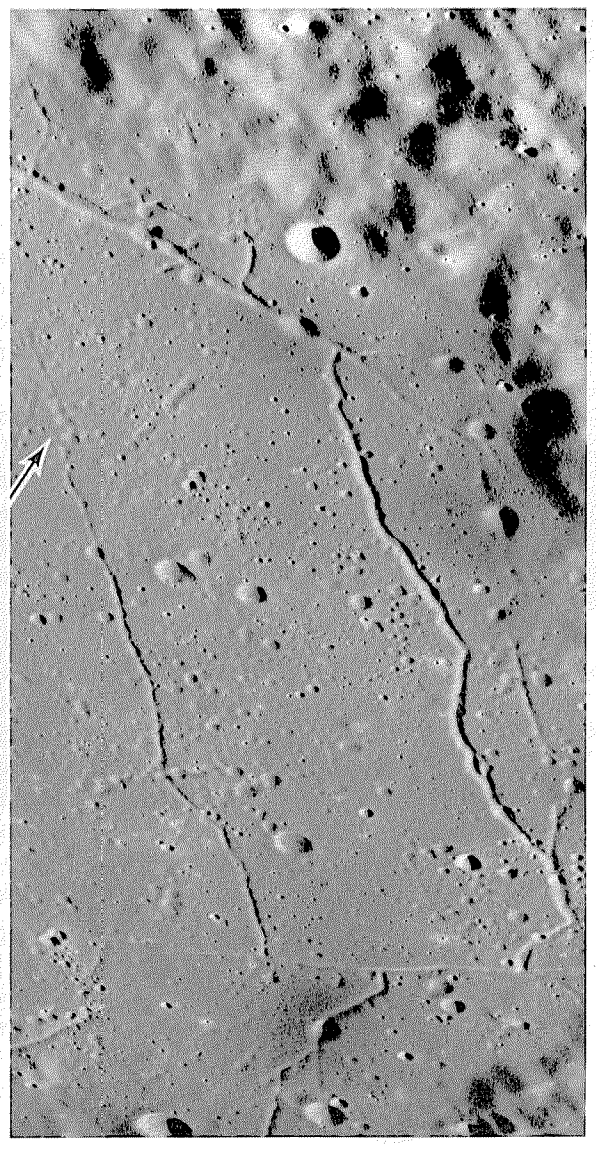

F

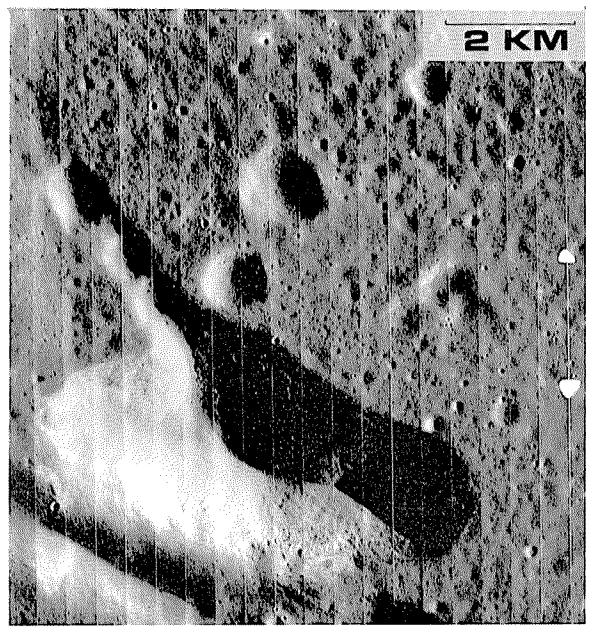

H

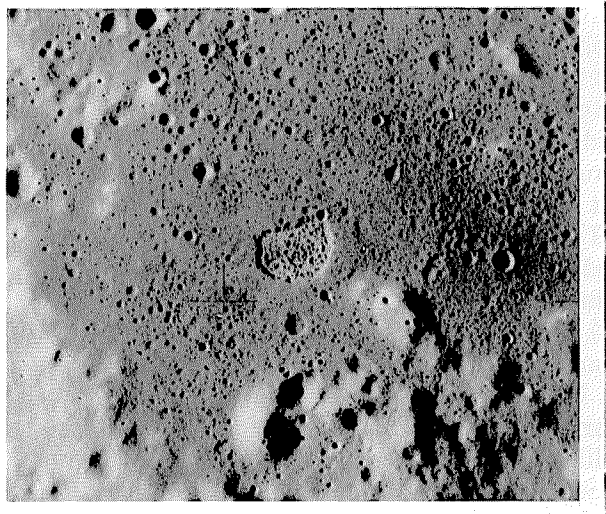

D

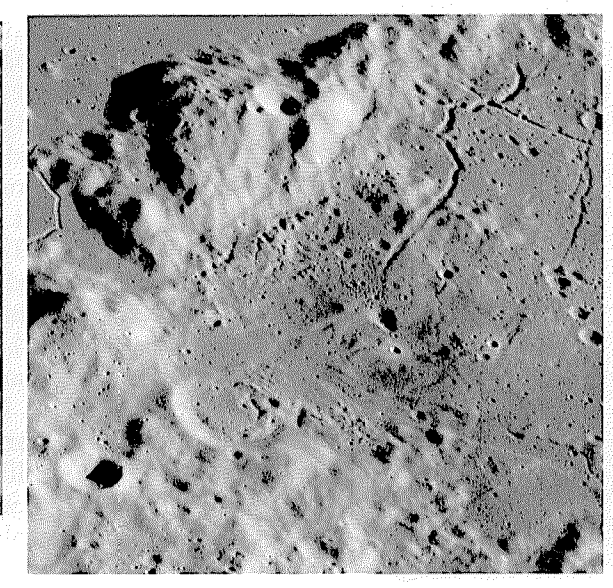

G

FIGURE 5.10.—Endogenic craters.

A. Craters aligned along graben on south margin of Mare Serenitatis (18° N., 26° E.; compare fig. 11.13) Apollo 17 frame P–2321.

B. Aratus CA (24.5° N., 11° E.), compared by Greeley (1973) to a volcanic crater in Idaho. Stereoscopic pair of Apollo 15 frames P–9350 (right) and P–9355 (left).

C. Probable collapse craters in southern Mare Imbrium; collapse of the deep, well-defined crater (5 km long) broke mare surface, whereas collapse of the gentler crater probably did not. Apollo 17 frame P–3125.

D. "D-caldera" (Ina), an irregular crater (3 km long) with peculiar floor texture. In Lacus Felicitatis (19° N., 5° E.), perched on Montes Apenninus flank, 300 to 400 m above nearest large mare (Vaporum; Strain and El-Baz, 1980). Apollo 17 frame M–1672.

E. Rima Hyginus; largest crater is Hyginus (9 km, 8° N., 6° E.). Orbiter 4 frame H–102.

F. Dark-haloed craters along fissures in floor of crater Alphonsus (compare fig. 1.8; Carr, 1969; McCauley, 1969a). Arrow (5 km long) indicates Ranger 9 impact point (12.9° S., 2.4° W.). Apollo 16 frame P–4656.

G. Irregular crater, fissure, and dark-mantling material (center) in Montes Riphaeus (6° S., 27° W.). Apollo 16 frame P–5453.

H. Crater next to Rima Bode II (13° N., 4° W.), amidst dark-mantling material (patch d3, fig. 5.14). Orbiter 5 frame H–122.

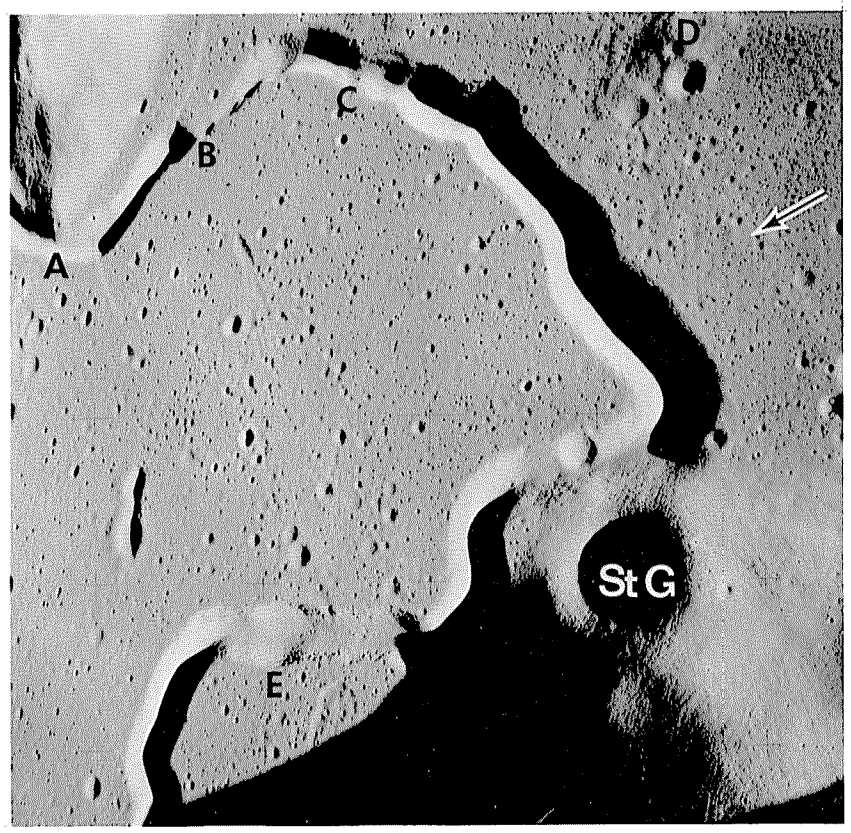

FIGURE 5.11.—Rima Hadley (Hadley rille) at Apollo 15 landing site (arrow). Rille hugs and possibly erodes terra at A, and is bridged at B and C by basalt. D, dark-mantled "North Complex," surrounded by level mare. Ledges are visible at E. StG, St. George Crater (2.25 km). Apollo 15 frame H–11720.

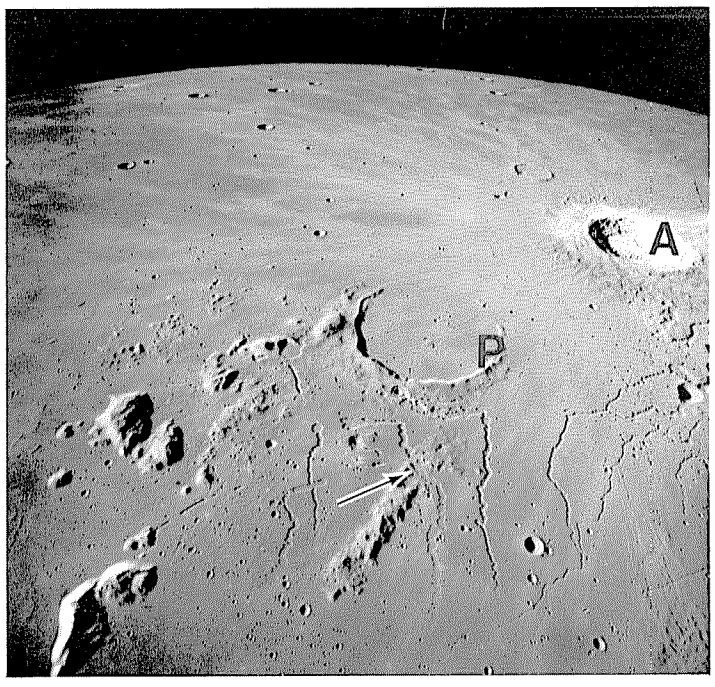

A

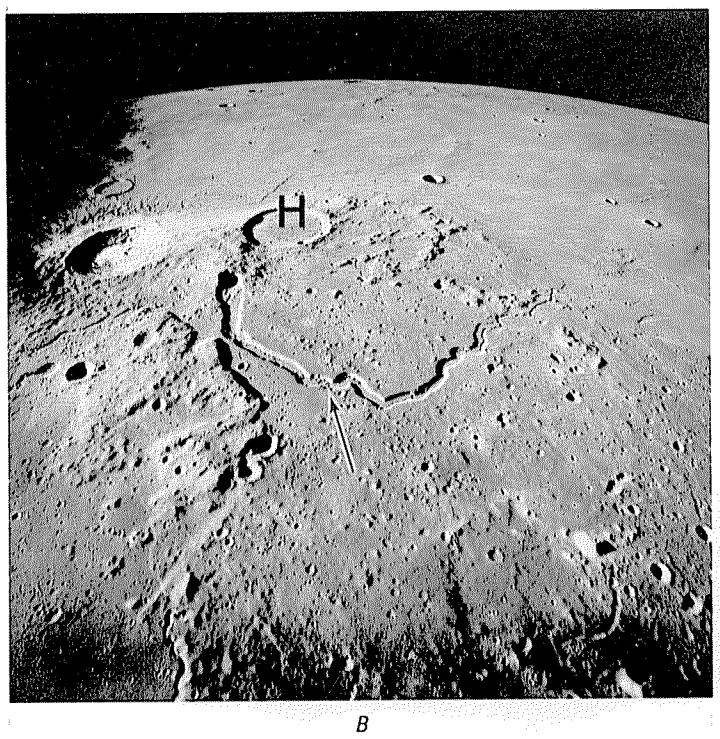

B

FIGURE 5.12.—Aristarchus Plateau-Montes Harbinger complex of sinuous rilles.

A. Montes Harbinger and crater Prinz (P). Large fresh crater is Aristarchus (A; 40 km, 24° N., 47° W.). Arrow indicates rille in *C*. View southward. Apollo 15 frame M–2606.

B. Aristarchus Plateau. Aristarchus is at left edge; H, Herodotus (35 km, 23° N., 50° W.). Arrow indicates rille in *D*. View southward. Apollo 15 frame M–2611.

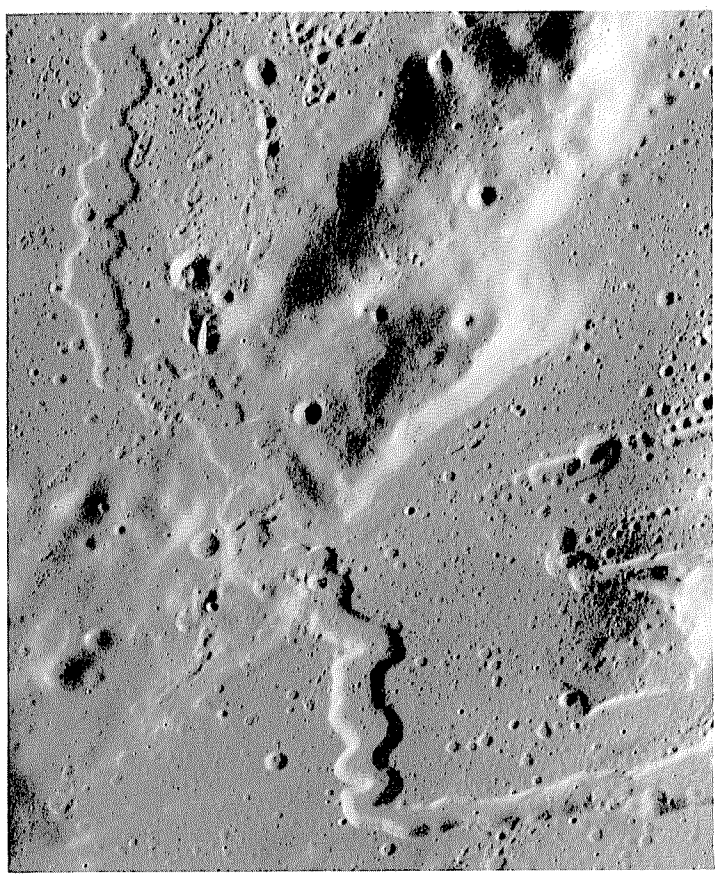

C

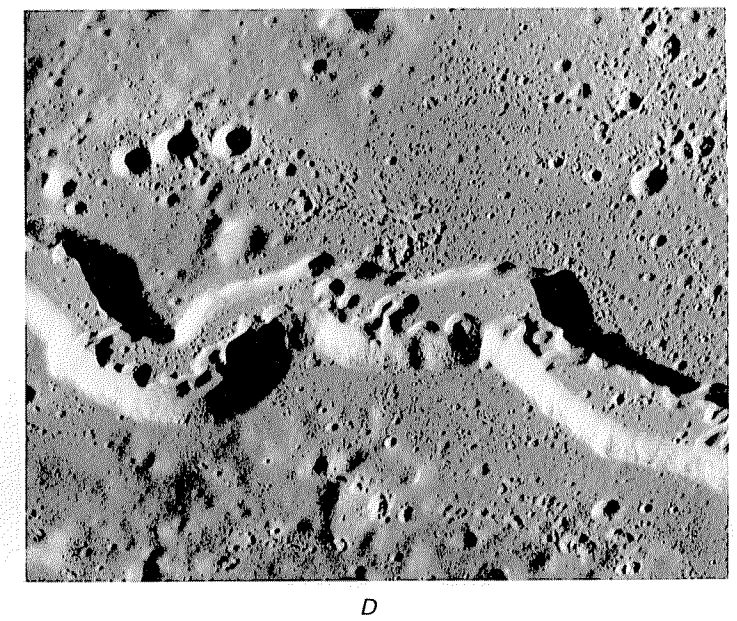

D

C. Terra ridge in Montes Harbinger (arrow in *A*), eroded by rille. Apollo 15 frame P–321.

D. Small meandering rille within largest lunar sinuous rille, Vallis Schröteri (arrow in *B*), which probably formed in massive lava flow(s). Apollo 15 frame P–341.

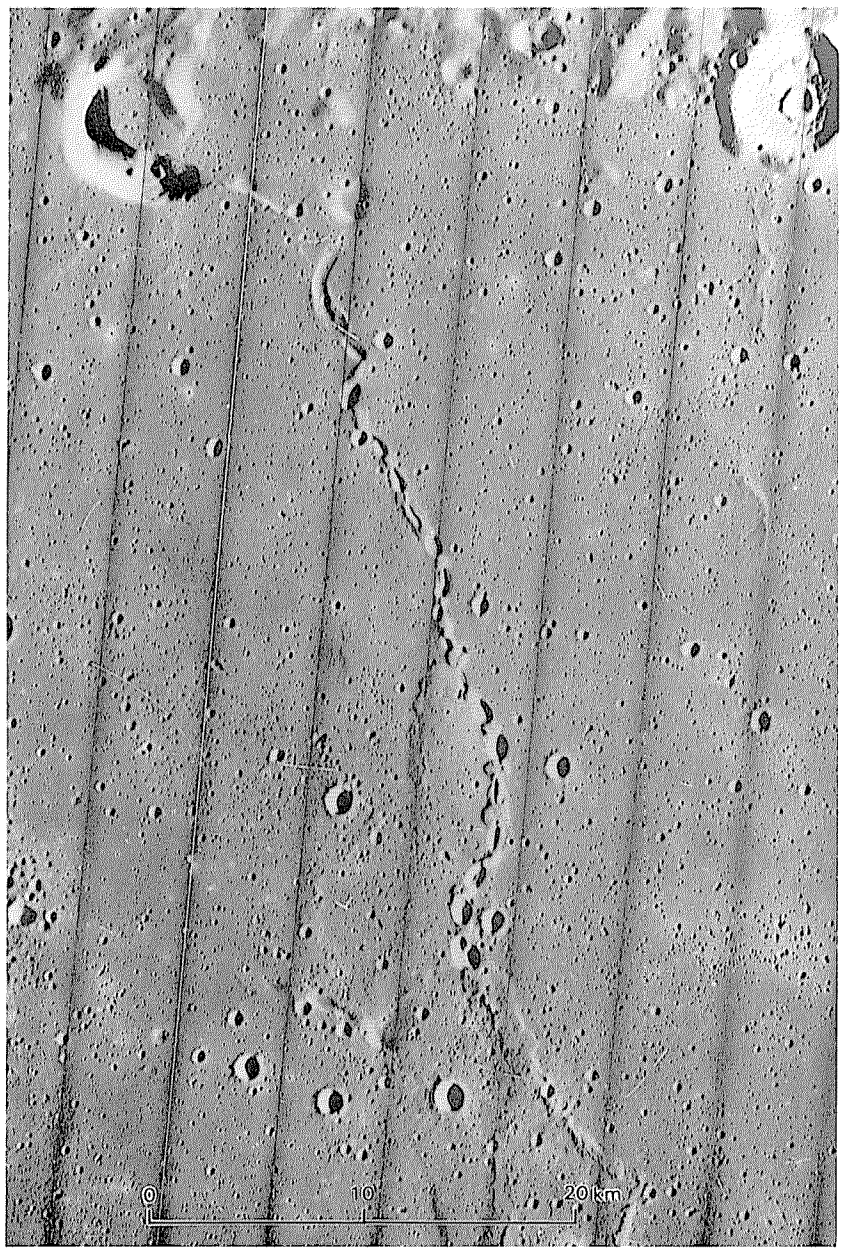

FIGURE 5.13.—Sinuous complex, consisting of ridge and elliptical and curved pits, that may have originated as a lava tube whose surficial crust collapsed intermittently along its length (Oberbeck and others, 1969). Crater in upper right corner is Gruithuisen K (6 km, 35° N., 43° W.). Orbiter 5 frame M–182.

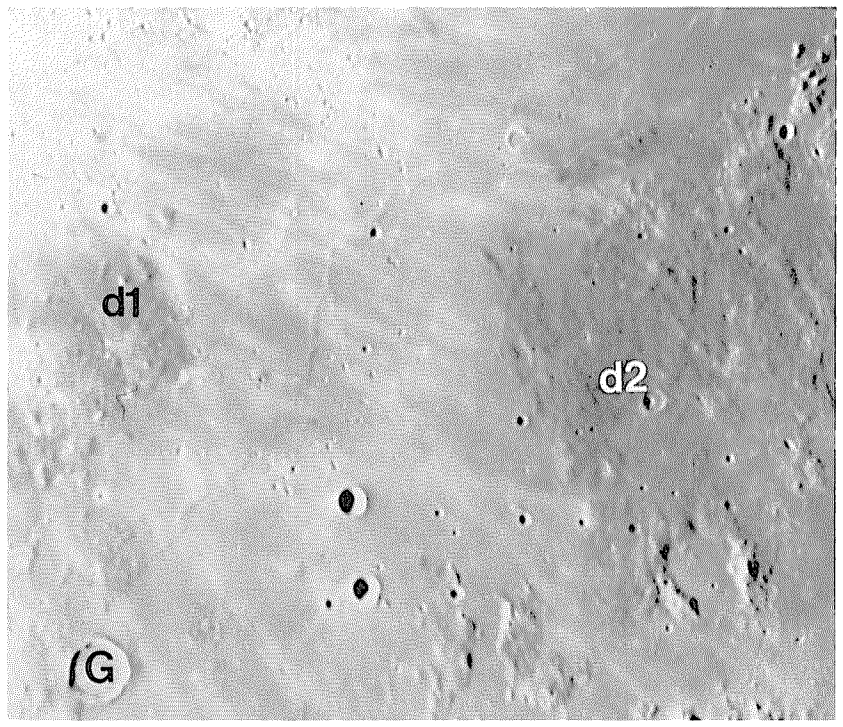

FIGURE 5.15.—Ray-crossed patch of dark-mantling material south of Copernicus (d1) and large patch south of Sinus Aestuum (d2; compare fig. 5.14). Sharp-rimmed (delta-rimmed) crater at lower left is Gambart (G; 25 km, 1° N., 15° W.; compare fig. 3.15C). Telescopic photograph.

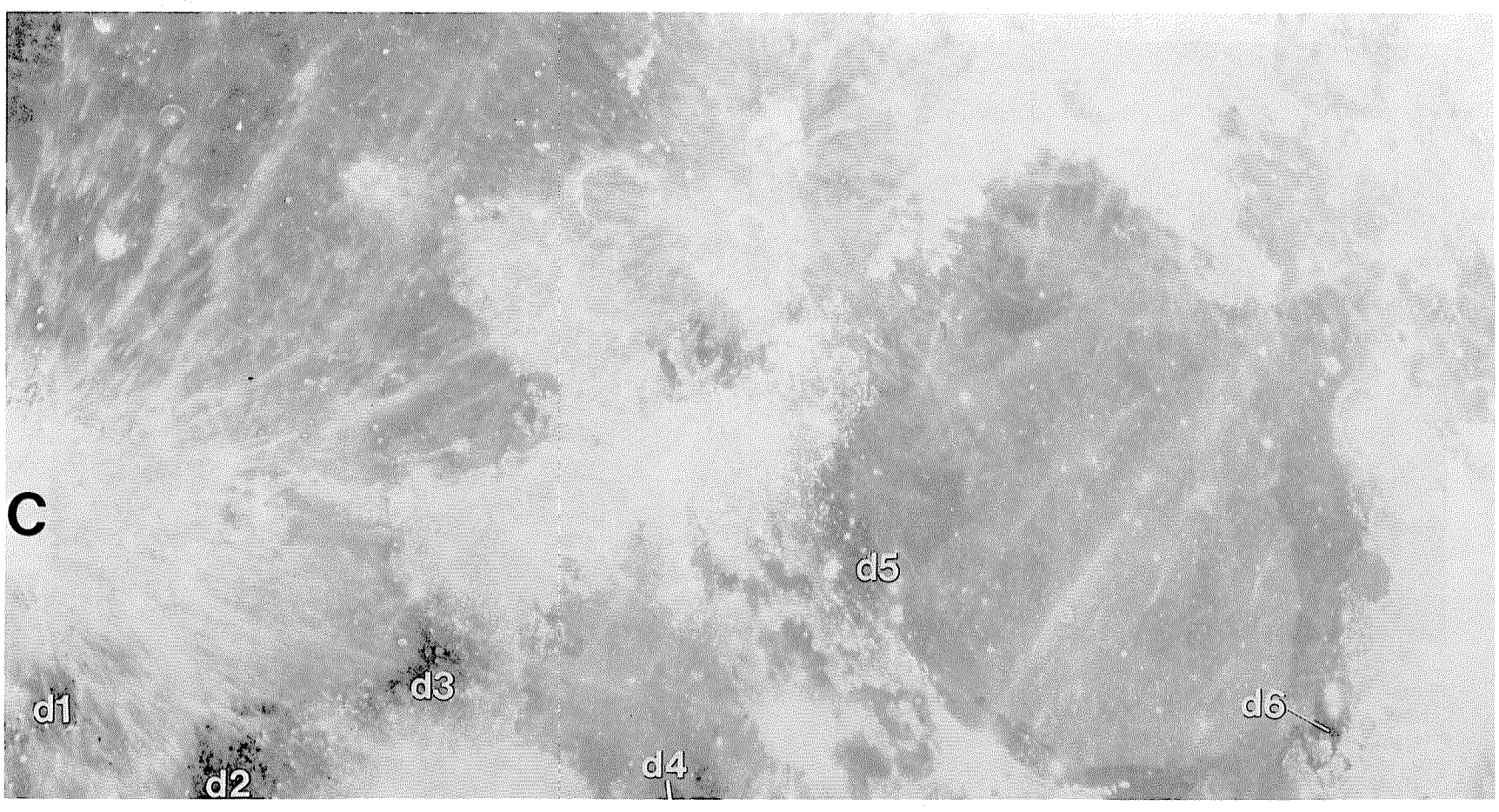

FIGURE 5.14.—Telescopic full-Moon photograph of Maria Imbrium (upper left) and Serenitatis (right). Bright crater Copernicus (C) is at left edge. Dark patches are south of Copernicus (d1), on border of Sinus Aestuum (d2, d3), on border of Mare Vaporum (d4), and along margin of Mare Serenitatis (d5, d6). Serenitatis is also bordered by other dark mare units. U.S. Naval Observatory, Flagstaff, Ariz., photograph.

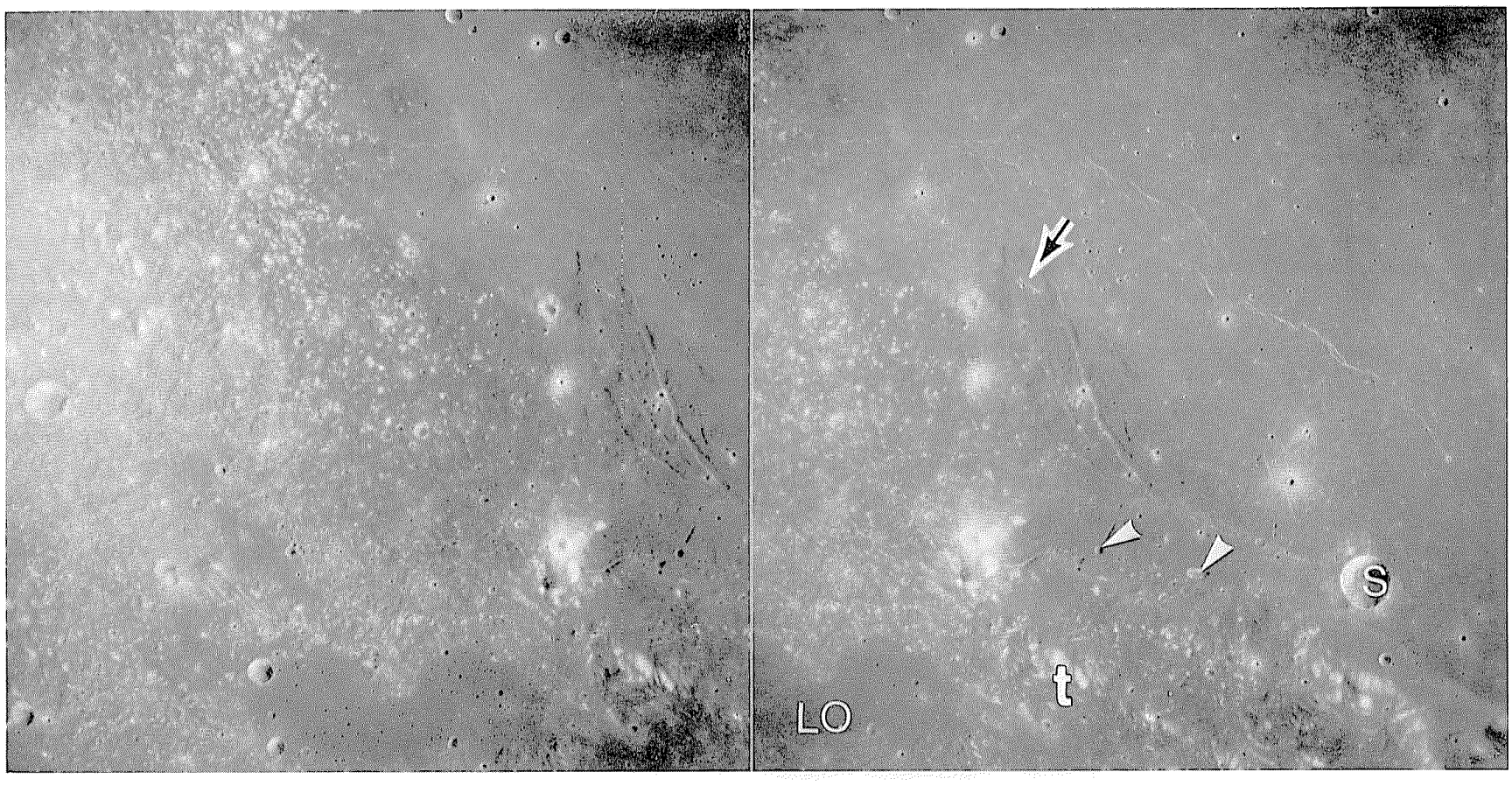

FIGURE 5.16.—Dark-mantling materials on southwest rim of Serenitatis basin (d5, fig. 5.14). Decrease in number of exposed bright terra peaks from lower left to upper right indicates increase in thickness of dark-mantling material toward the mare. Talus of dark-mantling material (t) covering brighter slope indicates shedding of superposed dark deposit. Black-and-white arrow indicates flooding of dark-mantling material by mare lava. Arrowheads denote endogenic craters. Lacus Odii (LO), which is elevated substantially (approx 1.5 km) above Mare Serenitatis, may consist of pooled dark-mantling material (Wilhelms, 1980). Arcuate rilles are Rimae Sulpicius Gallus; S, crater Sulpicius Gallus (12 km, 20° N., 12° E.). Stereoscopic pair of Apollo 17 frames M–2701 (right) and M–2703 (left).

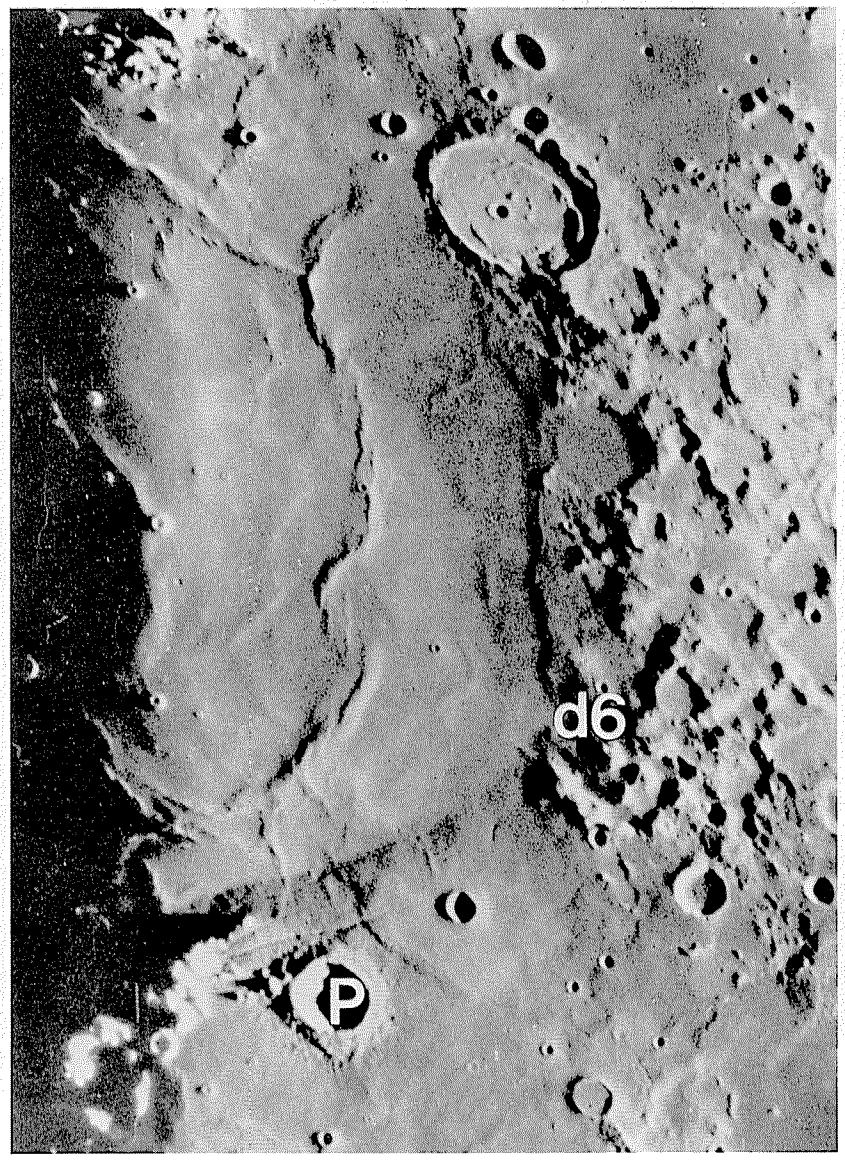

FIGURE 5.17.—Eastern Mare Serenitatis and adjacent terrain. Dark-mantling material (d6; compare fig. 5.14) is in region of Apollo 17 landing site. Central Serenitatis is depressed below darker border zone; grabens (see chap. 6) are in border zone above crater Plinius (P; 43 km, 15 N., 24 E.). Elevation of Mare Tranquillitatis (bottom) is approximately the same as that of Serenitatis border zone. Large crater Posidonius (95 km) along mare-terra contact near top of photograph has an uplifted floor (see chap. 6). Telescopic photograph.

Albedo

Because of the contrast between exposures of feldspathic terra breccia and mafic mare basalt, the maria can be delineated even by unsophisticated observations (figs. 1.1, 5.14). For example, Luna 3 was able to reveal the important fact that the farside is deficient in maria, despite poor camera resolution (Barabashov and others, 1961; Whitaker, 1963).

This observation illustrates that the mare-terra contrast shows up best when the Sun illumination is high; shadows become very rare, and true brightness differences are observed, at Sun angles higher than about 45°. The highest possible Sun angle, exactly normal to the surface, is called *zero phase*; the reflectance at zero phase is known as *normal albedo*. Zero phase is never observed from the Earth because the Moon would be eclipsed, and so quantities described by terms such as reflectance, reflectivity, brightness, or, simply, albedo are used more or less interchangeably as convenient approximations to true normal albedo. Mare albedos generally range from 0.07 to 0.10; that is, the maria reflect 7 to 10 percent of the incident visible light (Pohn and others, 1970). With minor exceptions, the total range of lunar visible albedos is about 0.07 to 0.24.

Considerable effort has been applied to quantifying albedo because of its value in distinguishing geologic units (Pohn and others, 1970). For geologic mapping of intramare units, however, high-Sun photographs with good spatial resolution are required, even if not accurately calibrated from region to region, because they show contacts between albedo units. Mare units have been extensively mapped since preparation of the geologic map of Mare Serenitatis (fig. 5.18; Carr, 1966a), where the boundaries are relatively unobscured by rays and the contrast between the dark border and the brighter interior is evident. Four Serenitatis albedo units became standards for mapping other areas (Wilhelms, 1970b, p. F30). Although the causes of these albedo differences were not known, the fact that albedo correlates to some extent with mare units was clear.

A leading hypothesis was that albedo is related to age. Several lines of evidence suggested that dark units are young and light units old. Except with respect to large craters (Dodd and others, 1963), the inward-sloping Serenitatis border mare appeared to contain fewer craters than the central mare. The dark-mantling materials of the border are superposed on some mare materials and appeared to be young. Dark-mantling or mare materials are superposed on lighter planar materials in other areas, for example, in Alphonsus, Mare

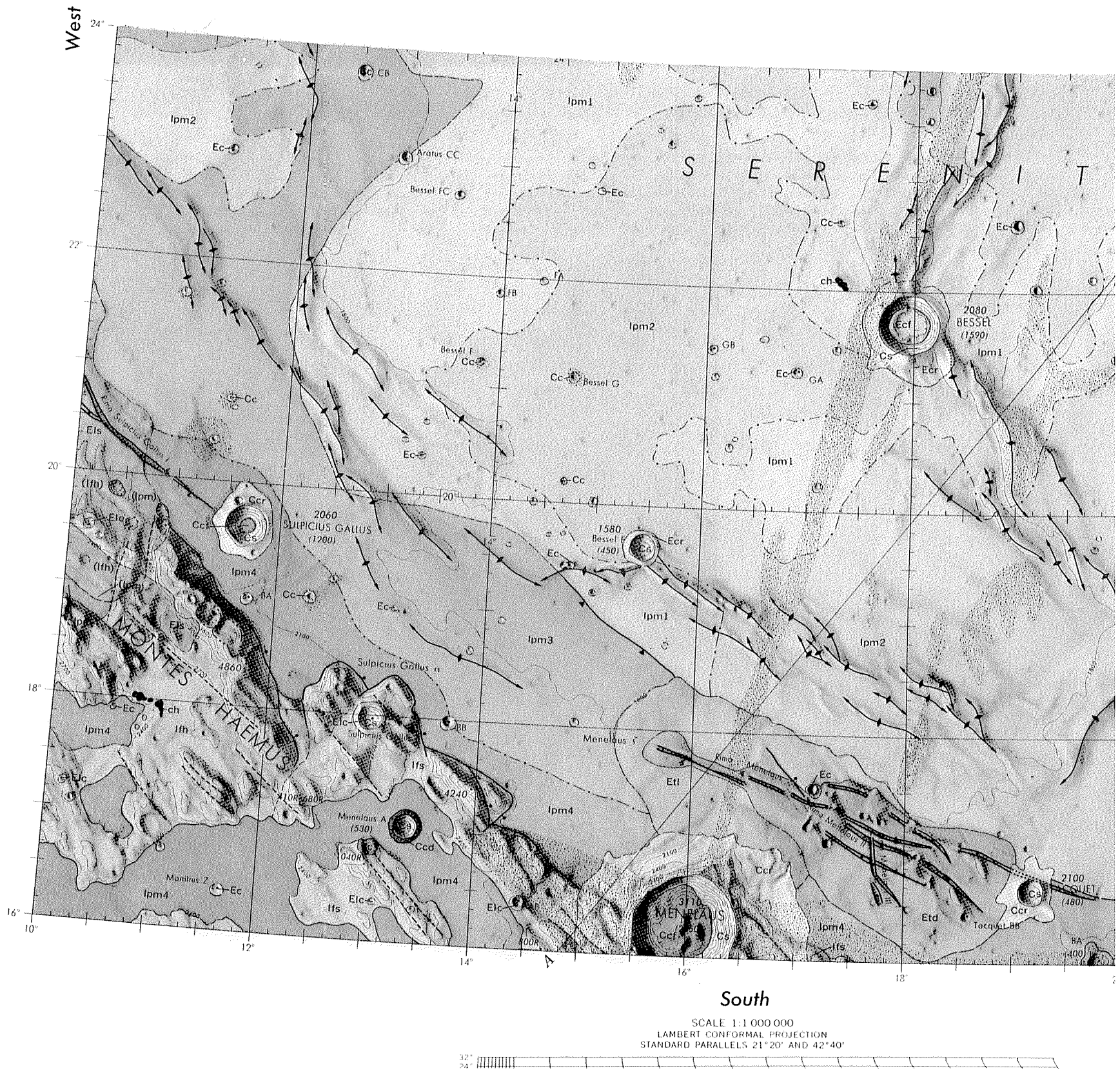

FIGURE 5.18.—Geologic map of Mare Serenitatis and margin (from Carr, 1966a). Dark mare (Ipm3, Ipm4) and dark-mantling materials (Emd, Els) of border zone are mapped in dark tones. High-numbered units were thought to be young; they actually are young in northeast and northwest, but are old in south. Unit boundaries remain valid.

Imbrium, Palus Putredinis, Julius Caesar, and Sinus Medii (figs. 1.6, 5.10*E*, *F*, 10.35, 11.13). Moreover, crater rays are generally brighter than the maria they cross, and so cratering was assumed to be an "instant aging" process that brightened materials. Correlation of albedo units thus became a means of correlating mare ages from area to area (Wilhelms, 1970b), and albedo units were shown as age units on most lunar geologic maps.

Albedo is now known to be more a function of composition than of age, as suspected by some geologic mappers (Trask and Titley, 1966). The dark basalt of the Mare Serenitatis border that was sampled by Apollo 17 yielded some of the oldest absolute ages yet obtained on exposed mare materials (see chap. 11). Albedo is a function of exposure to the space environment and of the alteration processes that create regoliths (soils) from bedrock. It is controlled by both the amount and the composition of glasses developed from crystalline material by small impacts (Adams and McCord, 1970, 1971, 1973; Nash and Conel, 1973). These glasses are darker than their parent crystalline materials. The most significant glasses in the darkening process are those that bind other regolith fragments into the complex aggregates known as *agglutinates*. Agglutinates accumulate in the regolith as a function of exposure age. Eventually, the amount accumulated reaches a steady state in which new micrometeorite impacts destroy as much agglutinitic material as they create. The albedo is then at an equilibrium value, and the regoliths are termed *mature* (Charette and others, 1974). The observable properties of mature regoliths are relatively homogeneous over the extent of a given bedrock unit.

In mature regoliths, the composition of the agglutinates strongly affects the albedo; regoliths highest in iron and titanium are the darkest (Adams and McCord, 1970, 1973; Pieters, 1978, p. 2839–2840). Because all undisturbed mare regoliths are believed to be mature, the darkest regoliths form from the lavas that are highest in Fe and Ti. Higher contents of these elements also explain why the maria are darker than the terrae. The darkening agents may be Fe-Ti-rich glasses, Fe and Ti oxides in such opaque minerals as ilmenite that are contained in the agglutinates (Pieters, 1978), and (or) metallic Fe reduced from oxides by impacts and solar-wind sputtering (Hapke and others, 1975). Although Fe may be the greater contributor to total darkening, the differences in albedo among mare units may be due more to differences in Ti content, because Ti content varies more among mare basalt units than does Fe content (Pieters, 1978, p. 2840). In other words, all mare regoliths are dark because their glasses contain Fe and Ti, but the darkest contain the most Ti.

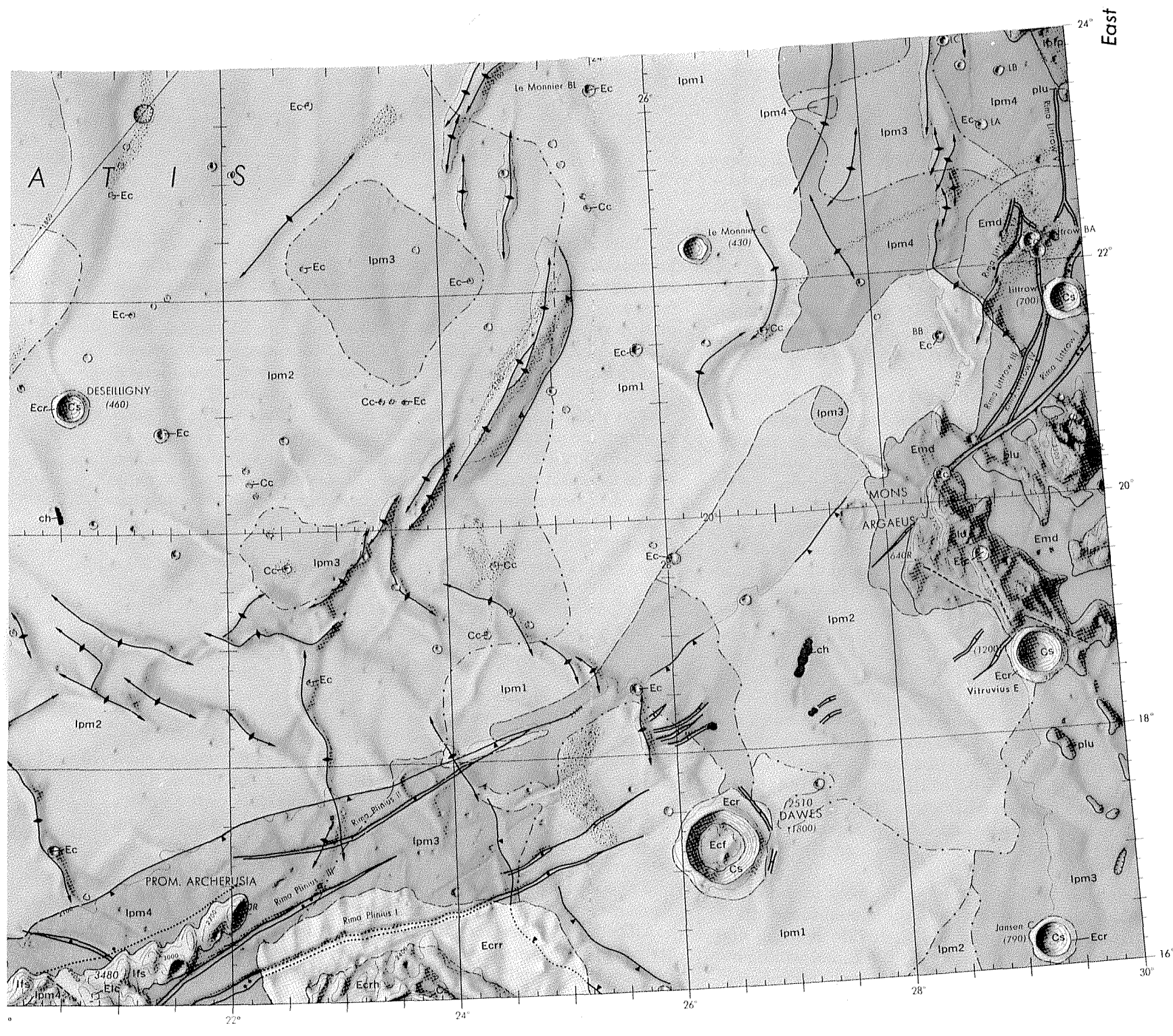

This correlation between darkness and Fe-Ti content applies only to mature regoliths. Fresh exposures of mare materials may not have been exposed long enough to accumulate impact glass in steady-state amounts. Such exposures occur in two main settings. First, new glass is shed, and nonglassy material continuously exposed, on steep slopes; the fresh material is brighter than the less disturbed material (figs. 3.28, 3.31, 5.16). In general, lunar slopes are brighter than adjacent more nearly level terrain composed of the same geologic unit (Shoemaker and Hackman, 1962). Second, relatively recent impacts exhume fresh material of mare lavas and redeposit it as bright rays. On bright, fresh lunar surfaces, more crystalline material than glass is exposed (Adams and McCord, 1970, 1971, 1973; Conel and Nash, 1970; Charette and others, 1974). Therefore, the formation of a crater ray in a given unit is not necessarily one of "instant aging" but of "instant rejuvenation." The correlation between youth and darkness demonstrated by dark-on-light superpositions is valid where the younger materials are richer in Fe and Ti, as in Alphonsus and the other examples given above, but not for all juxtapositions of dark and light.

In summary, geologic maps prepared before the mid-1970's correctly show relative ray and slope ages, and the mare units generally are correctly delineated. The mare units, however, should be interpreted as compositional, not age, units except where youth and composition correlate.

Color

Color differences are subtle on the Moon. The spectra of all areas are similar, and increase in reflectance toward longer wavelengths; that is, all lunar colors are red. Differences do exist, however, and can be detected with instrumented Earth-based telescopes and enhanced by various photographic, instrumental, and computerized image-processing techniques. Differences also appear conspicuous to the trained astronaut eye (Evans and El-Baz, 1973; Lucchitta and Schmitt, 1974). Color differences have proved to be valuable discriminators of lunar mare and dark-mantling units and, since the returned samples were analyzed, have helped extrapolate known compositions to unsampled units (table 5.1).

Reflectance spectra over wavelengths of 0.3 to 2.5 μm (ultraviolet to near-infrared) have been intensively studied during the space age for information about lunar compositions obtainable by remote means (fig. 5.19; Adams and McCord, 1970, 1973; McCord and others, 1972a, b, 1976; Adams and others, 1974; Charette and others, 1974; Pieters and others, 1974, 1975, 1980, 1982; Johnson and others, 1975, 1977; Head and others, 1978a, b; Pieters, 1977, 1978; Basaltic Volcanism Study Project, 1981, chap. 2). Areas 10 to 20 km across are measured photometrically. Absorption features due to mineral constituents of the surface material may be detected near wavelengths of 0.4, 1.0, 1.2, and 2.0 μm. These features are weak for agglutinate-rich regoliths and stronger for crystalline rocks (fig. 5.19*C*). To compare spectral differences, spectra are commonly divided by a standard spectrum of a relatively uniform mare surface in central Mare Serenitatis (designated MS–2; spectral class mISP, table 5.1). Small departures from this curve are then exaggerated in graphs, which are normalized to unity at 0.57 μm to eliminate albedo effects and to emphasize color differences (fig. 5.19). Most lunar spectra obtained before 1978 cover the spectral range 0.3 to 1.1 μm (figs. 5.19*A*, *B*; see references and historical background in Pieters, 1978, and Moore and others, 1980b). Spectra in the 1.0- and 2.0-μm bands have been obtained more recently (figs. 5.19*C*, *D*; McCord and others, 1981; Pieters and others, 1982).

For mapping and discriminating units, the most useful color-enhancement displays are images that show the spatial variations of simple spectral parameters (Whitaker, 1966, 1972b; Johnson and others, 1975, 1977; McCord and others, 1976). Black-and-white photographs prepared by combining a photographic negative taken at one wavelength with a positive taken at another provide much data at good spatial resolution (fig. 5.20; Whitaker, 1966, 1972b). Two major mare subdivisions, relatively red and relatively blue, can be defined. For example, Mare Tranquillitatis and the border of Mare Serenitatis are relatively blue, and central Serenitatis is relatively red. The young Imbrium flows are relatively blue, and most of the rest of Mare Imbrium is relatively red. Several intermediate colors can also be resolved.

TABLE 5.1.—*Remotely sensed properties of mare units*

[Spectral class from Pieters (1978) and Basaltic Volcanism Study Project (1981, chap. 2). Ultraviolet/visible ratio: H, high (probably more than 5 weight percent TiO_2); h, medium high; m, medium; L, low (probably less than 2 weight percent TiO_2). Albedo: D, dark (max 0.08); I, intermediate (0.03-0.09); B, bright (higher than approx 0.09); 1-μm absorption band: S, strong; G, gentle; W, weak. 2-μm absorption band: P, prominent; A, attenuated; -, undetermined.
Color (fig. 5.20): b, blue; i, intermediate; r, red.
Age (see chaps. 11-13): I1, earliest Late Imbrian; I2, middle late Imbrian; I3, latest Late Imbrian; E-I, near the Imbrian-Eratosthenian boundary; E, Eratosthenian; C?, Copernican (spectral class uncertain).
Interpretation based on Basaltic Volcanism Study Project (1981, p. 452-456)]

Symbol (pl. 4)	Spectral class	Mare	Color	Samples	Age	Interpretation
1	HDWA	Tranquillitatis, Serenitatis border.	b	Apollos 11, 17.	I2	Highest Ti.
2	HDSA	Procellarum-------	b	---	E, C?	High Ti, radioactivity, Fe?, olivine?
3	hDSA	Imbrium, N. Procellarum.	b	---	E	Similar to HDSA but probably lower Ti.
4	hDSP	Humorum, S. Procellarum.	b	---	E-I	Similar in Ti, Fe, and radioactivity to HDSA and hDSA, but possibly richer in pyroxene.
5	hDG-	Nubium----------	b	---	I3?	Medium Ti.
6	hDWA	Fecunditatis, Serenitatis border.	i	Luna 16	E, I3	Medium Ti, high Al.
7	mISP	Central Serenitatis, W. Procellarum.	r i	---	I3	Low to medium Ti. Possibly richer in Fe in Serenitatis than in Procellarum.
8	mIG-	Widespread--------	i, r	Apollo 12	E-I	Class of generally low- to medium-Ti basalt.
9	mBG-	Nectaris, S. Fecunditatis.	i	Apollo 16?	I2	Low Ti, high Al.
10	LISP	Crisium, Roris, Frigoris.	i, r	Luna 24	I1-I3, E.	Very low Ti, high Fe.
11	LIG-	E. Imbrium, W. Serenitatis.	r	Apollo 15	I3	Low Ti, high radioactivity.
12	LBG-	Somniorum, Mortis, Imbrium border, N. Procellarum, Nubium.	r	---	I1-I3	Very low Ti, probably high Al.
13	LBSP	Frigoris, Imbrium, Nubium.	r	---	I2-E	Low Ti, high in Fe or pyroxene, high radioactivity.

Such multispectral images contain considerable compositional information. To a first approximation, the excess of ultraviolet or near-ultraviolet color over the midvisual—that is, blueness—is a measure of the content of both FeO and TiO_2 in agglutinates within mature regoliths (Pieters, 1978, p. 2835). In figure 5.20 (made from photographs filtered at 0.37 and 0.61 μm), dark areas are bluer and thus richer in these elements. The reason for the correlation (Pieters, 1978, p. 2835–2841) is somewhat complex. As discussed, Fe and Ti darken mature regoliths, and the dark materials in the regolith suppress the intensities of individual absorption bands. The more Fe and Ti in pure glass, the more ultraviolet light is absorbed, that is, the redder the spectrum. The opposite can be observed, however, for many Fe- and Ti-rich mature regoliths, because dark regoliths containing well-developed agglutinates also strongly absorb in the visible and near-infrared. The resulting greatly reduced spectral contrast causes the apparent blue color of dark mature mare regoliths (Pieters, 1978).

Low Fe and Ti contents, however, do not necessarily cause the opposite effect. Red or intermediate-color maria are lower in Ti than relatively blue maria, but their Ti content is not constrained (Pieters, 1978, p. 2842–2843). The role of Fe in the red maria is unclear. The strength of an absorption feature near 1 μm is affected both by the Fe content of the regolith glass and by the proportion and composition of the mafic minerals present. This interrelation has not yet been fully examined (Adams, 1975; Pieters, 1978, p. 2840–2841).

The dark-mantling materials have distinctive reflectance spectra (fig. 5.19*D*; Pieters and others, 1973; Adams and others, 1974; Charette and others, 1974). Mantles that appear black on the surface or bluish-gray to an orbiting astronaut are spectrally blue as well, and those that appear orange on the surface or reddish-brown to tan from orbit are spectrally red. These colors are due to both the composition and the crystallinity of the pyroclastic dark-mantling materials. Some mantled regions differ spectrally from any sampled materials.

The bright interiors of fresh, young craters on both maria and terrae differ spectrally from the surrounding mature regoliths because their regoliths contain less agglutinitic material and more unaltered mineral fragments (fig. 5.19*C*). These properties affect the general properties of the spectral continuum and allow detection of specific near-infrared absorption features (Charette and others, 1974; Pieters, 1977). Visual wavelengths and, thus, the color-difference image in figure 5.20 do not fully reveal the spectral properties of fresh craters; these properties are better revealed by spectral images in the visible and near-infrared because of the conspicuous 1.0- or 2.0-μm absorption bands of pyroxene (fig. 5.19*C*; McCord and others, 1976).

Orbital chemistry

Two instruments flown in lunar orbit on the Apollo 15 and 16 missions have also permitted extrapolations of sample compositions to unsampled parts of the Moon. The gamma-ray spectrometer and X-ray-fluorescence spectrometer Adler and Trombka, 1977; Basaltic Volcanism Study Project, 1981, chap. 2) are currently the only means of estimating compositions on the farside (pl. 2). Whereas the reflectance spectra help determine mineral and glass contents, the two orbital instruments determine elemental compositions independently of mineralogy.

The compositions determined are those of only the surficial layers, the uppermost tens of centimeters in the case of the gamma-ray data and the uppermost tens of micrometers for the X-ray data. Investigators are nevertheless confident that most surficial regolith materials represent underlying materials because the sharp bound-

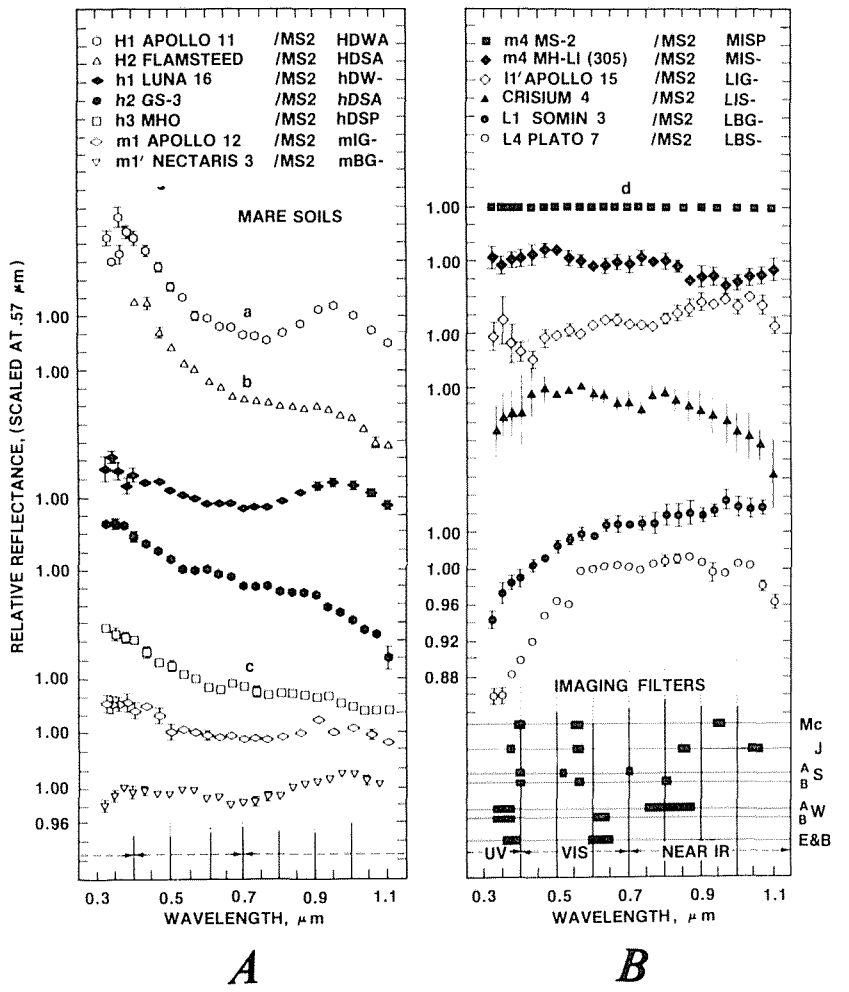

A *B*

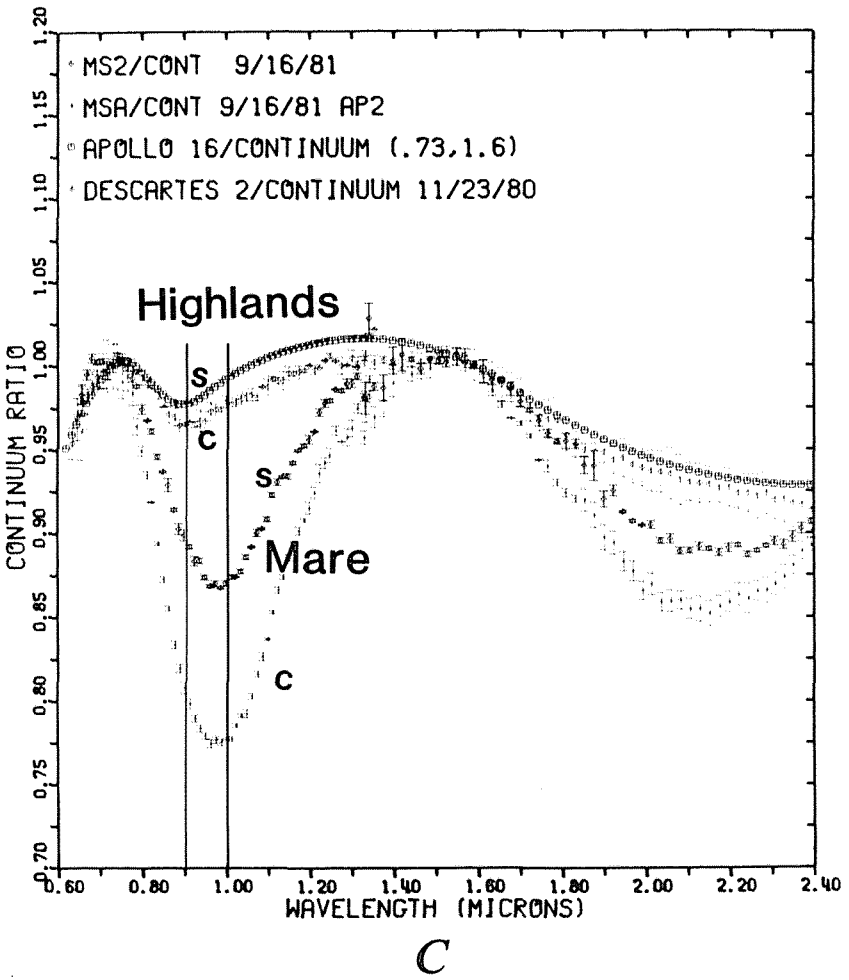

C

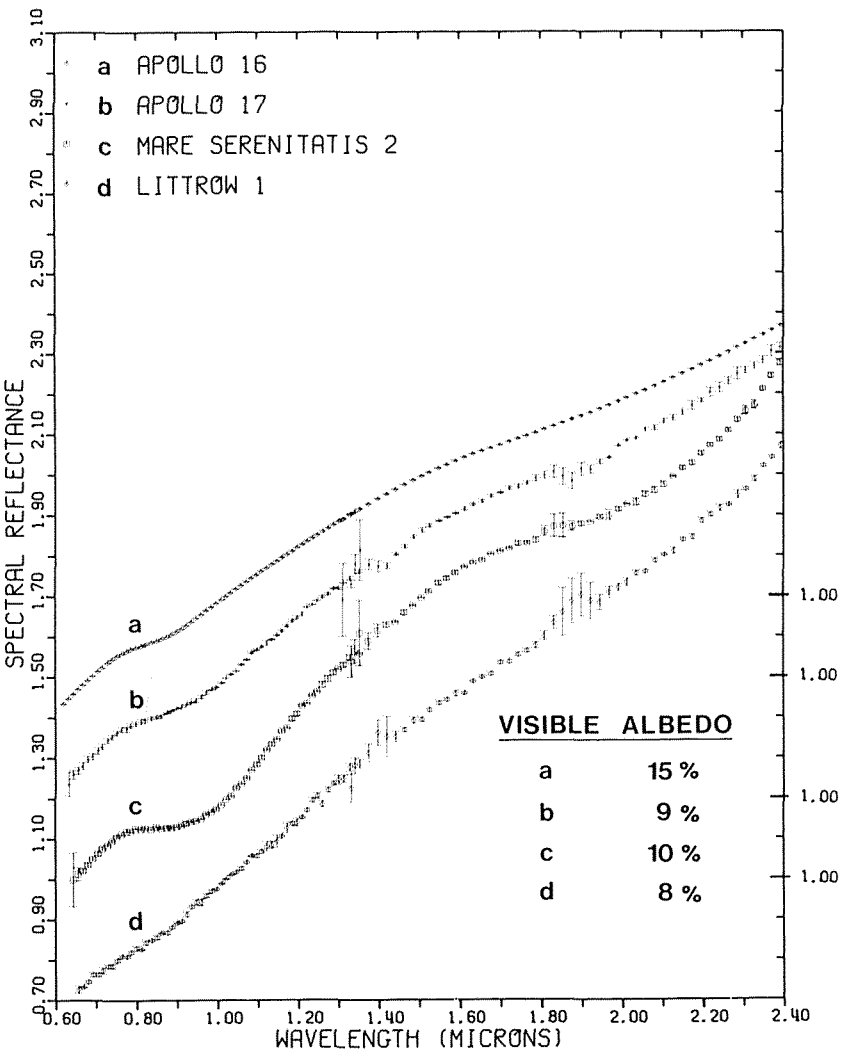

D

FIGURE 5.19.—Typical relative-reflectance spectra of lunar soils (surficial fine materials of regoliths) obtained by Earth-based telescopes. Courtesy of C.M. Pieters.

A. Spectra of mare soils between 0.3 and 1.1 μm, relative to an area in central Mare Serenitatis (MS2 or MS–2) and scaled to unity at 0.57 μm. Designations to left of area names are from classification of Pieters and McCord (1976), and those to right (see table 5.1) are from Pieters (1978). After Pieters (1978, fig. 3).

B. Additional mare spectra of same type. Slopes of plots emphasize differences of spectra from that of comparison area MS–2 (horizontal). Bandpasses of filters used in various spectral-imaging studies are shown at bottom (see Pieters, 1978, fig. 3).

C. Near-infrared spectra of areas 5-10 km across, scaled to unity at 1.02 μm and divided by a straight-line continuum. For a given terrane (highland or mare), spectra of soils (s) and interiors of fresh craters (c) are qualitatively similar, but spectral contrast of soil spectra is reduced by alteration products in the soils. Absorption bands of highlands are centered near 0.90 μm, indicating that Ca-poor pyroxene is the dominant mafic mineral; absorption bands of maria are near 0.98 μm, indicating that Ca-rich pyroxene is the dominant mafic mineral.

D. Spectra in the visible and near-infrared, scaled to unity at 1.02 μm: a, terra soil around Apollo 16 landing site, calibrated with returned soil sample 62231; b, Apollo 17 landing site, a Ti-rich basaltic soil; c, standard area MS2, probably a low-Ti basalt; d, pyroclastic dark-mantling material near the Apollo 17 landing site.

aries between mare and terra and among mare units, as seen on the color-difference images (fig. 5.20), have persisted since the maria formed (Kuiper, 1965, p. 13). Small fragments of nonlocal material are present in all regoliths, though not in sufficient quantity to mask the local material.

The gamma-ray spectrometer measures the natural radioactivity of K, Th, and U, as well as gamma rays emitted from other elements during nuclear reactions induced by high-energy cosmic-ray bombardment (Metzger and others, 1973, 1977; Adler and Trombka, 1977; Reedy, 1978; Basaltic Volcanism Study Project, 1981, chap. 2). The most useful results are obtained for concentrations of Th, K, Fe, Mg, and Ti (Bielefeld and others, 1976; Metzger and others, 1977; Haines and others, 1978; Metzger and Parker, 1979; Davis, 1980; Haines and Metzger, 1980). The Ti values obtained by the gamma-ray and spectral techniques agree moderately well (Basaltic Volcanism Study Project, 1981, p. 453). The gamma-ray spectrometers were limited by low spatial resolution, from 2° by 2° (3,600 km^2) to 10° by 10° (90,000 km^2) of the lunar surface; they analyzed about 22 percent of the total surface. On the basis of this areal sample, the maria are generally more radioactive than the terrae, and the western nearside maria more radioactive than the eastern (Soderblom and others, 1977).

The X-ray spectrometer detects the elements Al, Mg, and Si from the intensity of secondary X-ray fluorescence induced by solar X-rays (Adler and others, 1972; Adler and Trombka, 1977). Thus, the data are limited to illuminated parts of the lunar surface, and interpretations of the data must compensate for variations in solar activity. In all, about 10 percent of the lunar surface was analyzed. The Mg/Al ratio is most sensitive to terra-mare differences because it is substantially greater for mare materials, whereas Si content differs little between the maria and the terrae. Highly magnesian and highly aluminous mare and dark-mantling materials are also detectable by this ratio, other factors being equal (Andre and others, 1977, 1979a; Schonfeld and Bielefeld, 1978; Conca and Hubbard, 1979; Hubbard, 1979). Suitable data analysis has resolved areas as small as about 1° by 1° (900 km^2). At these resolutions, ejecta of individual craters and, therefore, the subsurface materials exhumed and redeposited in the ejecta can be analyzed (Andre and others, 1975, 1978, 1979b).

Other properties

Two other regions of the electromagnetic spectrum, accessible from the Earth or with the aid of a spacecraft, have potential value in interpretations of the maria. The first region, in the thermal infrared,

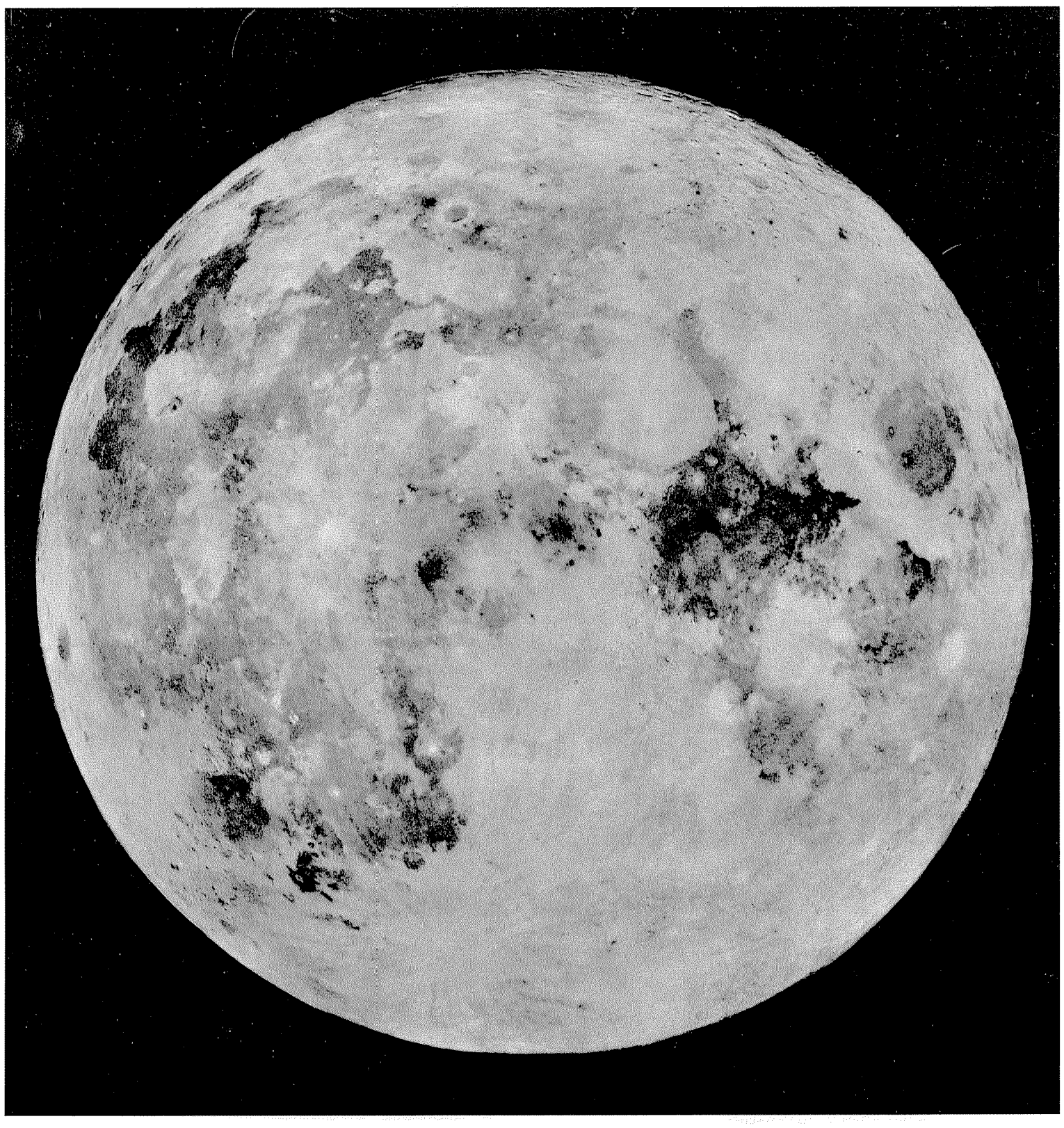

FIGURE 5.20.—Color-difference image, produced by subtracting photograph taken at 0.37 μm from one taken at 0.61 μm. Longer wavelengths (red) appear brighter and shorter wavelengths (blue) darker. Courtesy of E.A. Whitaker.

measures temperatures during a total eclipse of the Moon (Saari and others, 1966; Shorthill and Saari, 1969; Shorthill, 1973) or from orbit (Mendell and Low, 1975; Schultz and Mendell, 1978). High eclipse temperatures are valuable indicators of fresh blocky surfaces and thus of youthful craters, which may be undetectable in low-resolution photographs (see chap. 13; Winter, 1970; Thompson and others, 1974). For mare units, there seems to be a correlation between high eclipse temperatures and the youth of a unit (Moore and others, 1980b, p. B65). The knowledge gained from craters suggests that this correlation results from the coarse, blocky regoliths that thinly cover young mare units.

Lunar applications of radar have been intensively studied. Earth-based signals at 3.8 and 70 cm have yielded the most detail, including radar maps of the whole nearside disc (Zisk and others, 1974; Thompson, 1974, 1979; Moore and others, 1980b, p. B52–B61). Many factors affect radar echoes (Moore and others, 1980b, p. B53). For geologic purposes, the echoes ideally would measure depth of penetration and surface roughness at scales proportional to wavelength—larger than 70 cm for 70-cm radar and larger than 3.8 cm for 3.8-cm radar. Chemical composition, dielectric constant, electromagnetic absorption, fine-scale roughness, and regional tilt may all additionally affect the echoes. Despite the difficulty of interpretation, radar in combination with other remote-sensing techniques is a useful measure of crater youth: Depolarized radar echoes from craters decrease with decreasing concentrations of blocks visible in photographs and with decreasing infrared eclipse temperatures (Thompson and others, 1974, 1980). Radar data, infrared eclipse temperatures, and distinctive color spectra together help characterize mare units (Schaber and others, 1975; Moore and others, 1980b) and reveal the presence of block-free dark-mantling materials that might otherwise be taken for lava (Zisk and others, 1977).

During the Apollo 14, 15, and 16 missions, radar signals were relayed to and from the Moon by orbiting satellites (Moore and others, 1980b, p. B34–B41). Though technically highly successful, this "bistatic" radar experiment generated little new scientific information beyond the fact that bistatic-radar roughness correlates with the visual appearance of a terrain. Young mare units are rougher to radar than older mare units.

Integration

The examples already given show that remote-sensing techniques are most valuable when used in concert. Correlations among data sets are readily visualized when converted to a common format and displayed as false-color images showing any desired weighted combination of the data sets (Eliason and Soderblom, 1977; La Jolla Consortium, 1977; Soderblom and others, 1977). Geologic mapping requires images with good spatial resolution, including low-Sun images that enhance topographic detail, high-Sun photographs that show brightness differences (figs. 1.1, 5.14), and multispectral images (fig. 5.20). To characterize chemical and physical properties not determinable from such images, lower-resolution data from other measurements are located within each resulting map unit and then extrapolated to the entire area it covers.

Generalizations based on integration of the data, to be discussed further in chapters 11 through 13, include:

1. The western maria in the overflown strips are more highly radioactive than the eastern.
2. Ti-rich, spectrally blue lavas form at least half of Mare Tranquillitatis, the adjoining border of Serenitatis, the lobate flows of Mare Imbrium, central Mare Humorum, and much of Oceanus Procellarum. Most of these lavas are in maria that overlie the central basin and middle trough of the Procellarum basin (pl. 4). The Tranquillitatis-Serenitatis units, which include the Apollo 11 and 17 landing sites, belong to a different high-Ti spectral class (HDWA) than do the western units (HDSA, hDSA, hDSP).
3. Class hDWA occurs at several mare margins and fills most of Mare Vaporum. On the color-difference photographs, its color appears to be intermediate between red and blue and has been called "orange" (Basaltic Volcanism Study Project, 1981, p. 237). A patch at the Fecunditatis margin includes the Luna 16 landing site.
4. Red spectral classes, thought to be lowest in Ti content, are concentrated in Lacus Somniorum, Mare Frigoris, Sinus Roris, and northern Mare Imbrium; that is, they occur in diverse settings over the north half of the Procellarum basin. Apollo 15 landed within one of these classes (LIG-). Red or orange class LISP also occurs in Mare Crisium, where it probably underlies the Luna 24 landing site.
5. Red spectral class mISP forms extensive areas in central Serenitatis and the outer trough of western Procellarum. These two occurrences may differ in composition (table 5.1); they were not sampled.
6. Orange or (partly) red spectral class mIG- covers much of the area west of the central meridian and south of the strong blue-red association in Mare Imbrium. Apollo 12 landed within this belt. This class also forms much of Mare Crisium and Mare Fecunditatis. These concentrations may have little significance, however, because class mIG- is a group of low- to medium-Ti mare units that may differ compositionally (Pieters, 1978).
7. One interpretation of the orbital geochemistry is that Maria Smythii, Fecunditatis, and Crisium are all Al-rich (Conca and Hubbard, 1979; Hubbard, 1979). Orange spectral classes mBG-, characteristic of Mare Nectaris, and LBG-, common among the northern very red units, also are probably Al-rich (C.M. Pieters, oral commun., 1982).

THICKNESS

Recognition that the lunar mare surfaces are underlain by three-dimensional deposits led early to measurements of their thickness. Marshall (1961) estimated thicknesses in Oceanus Procellarum from the degree of obliteration of flooded craters, whose preburial profile was assumed to equal that of fresh craters of the same diameter (Baldwin, 1949, p. 128–138). Baldwin (1970), Eggleton and others (1974), and De Hon (1974) refined this method on the basis of better data for the profiles and rim dimensions. Mare-basalt thicknesses, including thicknesses of individual flows, also subtly affect the size-frequency distributions of craters (Eggleton and others, 1974; Neukum and others, 1975a). R.A. De Hon and his coworkers systematically extended these measurement techniques to most of the nearside maria (fig. 5.21). They found that the eastern mare materials average 200 to 400 m in thickness (De Hon and Waskom, 1976) and the western closer to 400 m (De Hon, 1979). Lenses thicker than 1,200 or 1,500 m also occur; more accurate values are hard to determine because few craters are visible in such thick mare sections (De Hon, 1979).

The accuracy of other mare-thickness determinations is uncertain. On the one hand, thicknesses will be overestimated if the craters on which they are based were highly degraded or filled before the mare flooding (Hörz, 1978), or if they have been shallowed by floor uplift (as is, in fact, observed in basins; see chap. 6). Hörz (1978) estimated that De Hon's figures are a factor of 2 too high. On the other hand, thicknesses will be underestimated if the craters are perched on older mare materials. Head (1979a) pointed out that the flooding of the present central highlands of the nearside, which must resemble the floors of some of the older basins, would require more mare material than believed by either De Hon (1979) or Hörz (1981).

A few geophysical determinations of thickness are available. The gravity data are consistent with thicknesses of 2 to 4 km in the centers of mascon maria (Sjogren and others, 1974; Solomon and Head, 1979, 1980), the largest of which are Imbrium, Serenitatis, Crisium, Humorum, Smythii, Nectaris, and Orientale (fig. 5.22; table 6.1; Solomon and Head, 1980). Large nonmascon maria include Tranquillitatis, Fecunditatis, and most of Procellarum. The 20- to 25-km-deep seismic discontinuity under Oceanus Procellarum was first interpreted as the base of the basalt section (Toksöz and others, 1974) but is now thought to represent a physical or chemical discontinuity within the terra crust (see chaps. 1, 8). Most of the mare fill of northern Oceanus Procellarum is thinner than 500 m. However, in one place in the north and in several places in the south, it reaches thicknesses greater than 1,000 m where superposed basins or large craters deepen the original Procellarum-basin floor (De Hon, 1979).

A radar sounder flown on the Apollo 17 mission directly measured depths to discontinuities in two mascon maria, Serenitatis and Crisium (Peeples and others, 1978). If certain assumptions about the dielectric constant of the overflown materials are correct, one horizon in Mare Serenitatis lies about 1 km beneath the surface, and another 1.6 km deep in the west to 2.0 km deep in the east (Peeples and others, 1978). One horizon apparently within the basalt section of Mare

Crisium lies 0.8 to 1.0 km below the surface of the shelf that separates the conspicuous ridge system and the basin rim (figs. 4.9, 5.23; Maxwell and Phillips, 1978; Peeples and others, 1978). What appears to be the same interface (Maxwell and Phillips, 1978) is 1.4 km deep inside the shelf.

Mare thicknesses have also been inferred from the geochemical experiments (Andre and others, 1979b). The craters Peirce (19 km) and Picard (23 km) penetrated the 1.4-km-thick layer in Crisium and excavated additional basalt whose Mg-rich chemistry is evident in the X-ray data (fig. 5.23*B*; Andre and others, 1978, 1979a, b). These craters may have excavated terra materials from beneath the mare (Head and others, 1978a). On the basis of assumed excavation depths, the total mare thickness in Crisium may be 2.4 to 3.4 km (Maxwell and Phillips, 1978).

Progressive decrease in the number of visible premare craters, the gravity data, and the radar-sounder profiles indicate that the mare materials are thickest in the mare centers (Baldwin, 1970). This relation reflects the topography of the host basin: Each concentric shelf of a basin is lower than the surrounding one, and the center is the lowest of all (chap. 4; figs. 4.9, 5.16, 5.17, 5.23). Elevations of the mare surfaces also mimic this step structure to some degree. For example, Mare Crisium lies about 2 km lower than peripheral Mare Spumans and 3 km lower than Mare Undarum (fig. 4.9). However, the mare surface drops in elevation less than the basin floor because of the inward mare thickening.

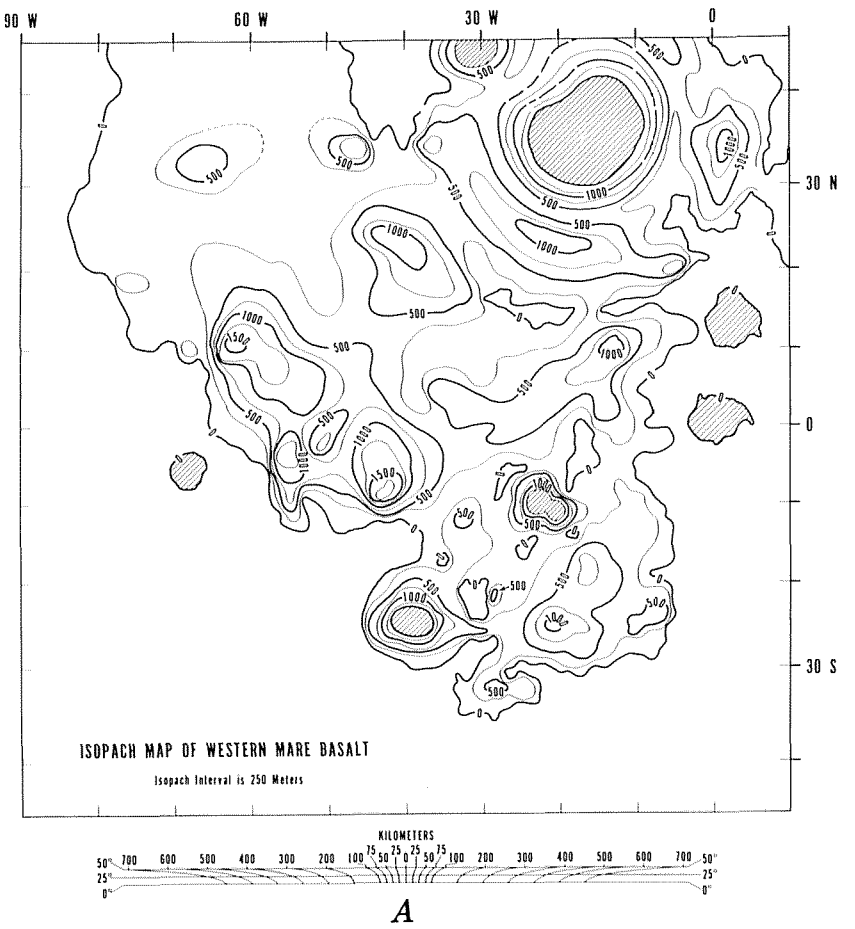

FIGURE 5.21.—Thickness of mare materials on western (*A;* De Hon, 1979) and eastern (*B;* De Hon and Waskom, 1976) nearside.

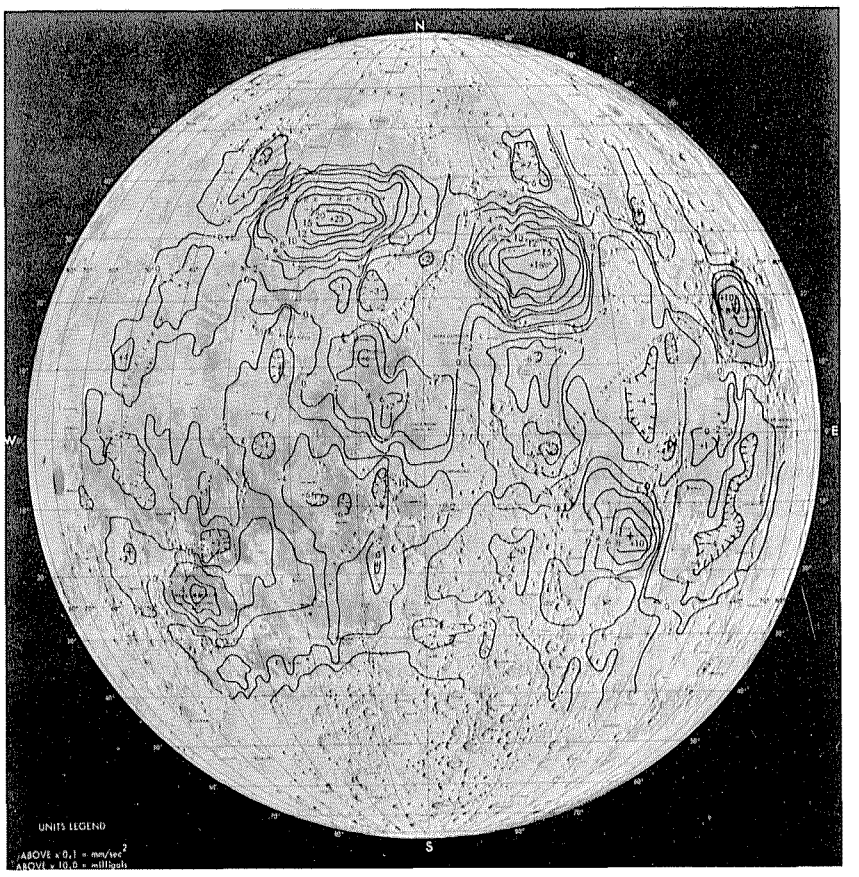

FIGURE 5.22.—Lunar gravity anomalies (from Muller and Sjogren, 1968).

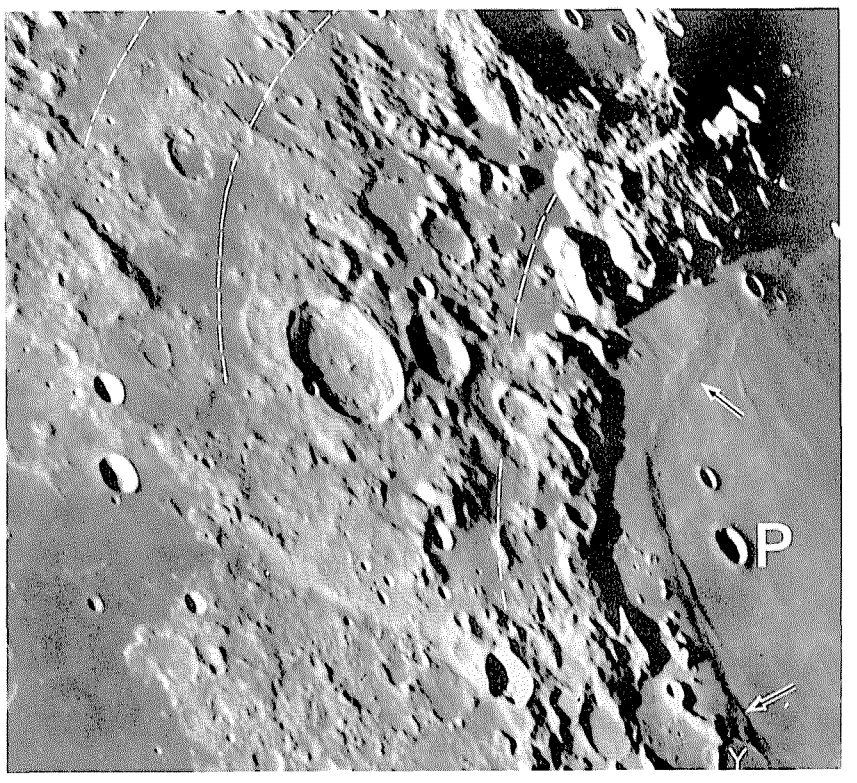

FIGURE 5.23.—Thickness of mare-basalt flows in Mare Crisium.

A. Western Mare Crisium and part of Crisium basin, showing difference in elevation (arrows) between mare shelf and depressed center. P, crater Peirce (19 km, 18° N., 53.5° E.). Dashed lines indicate basin-concentric troughs, as interpreted by Wilhelms (1970b). Telescopic photograph.

B. Diagrammatic cross section of Mare Crisium, based on radar-sounder profile (Peeples and others, 1978). Arrow denotes shelf indicated by arrows in *A*. Crater P (Peirce; also Picard) penetrates younger mare unit and excavates older mare unit (Mg-rich; Andre and others, 1978) and, possibly, terra underlying the mare section (Head and others, 1978a). Scales are diagrammatic, exaggerated vertically.

In summary, enough mare thicknesses have been measured to indicate that mare basalt is volumetrically minor. Few depths are likely to exceed 4 km; the thickest sections are in the centers of the circular maria. Thicknesses on mascon-mare shelves and nonmascon maria are no more than about 0.5 km. Likely lower and upper limits for the average mare-basalt thickness on the whole Moon are probably 0.2 and 1.0 km, respectively. Thus, the upper 75 km of the Moon would consist of 0.24 percent mare basalt if the average thickness is 1.0 km, and of only 0.047 percent if it is 0.2 km (based on coverage of 17 percent of the total lunar area of 38×10^6 km^2). Subsurface dikes and sills would add an unknown volume to these small values.

RETURNED SAMPLES

Introduction

The samples of basalt returned from the lunar maria present fewer problems than do those of breccia from the terrae, because most lavas acquire their chemical and physical properties when their magmas originate and when they are emplaced, and not from an earlier geologic unit. Most rock-size basalt samples are not shock-melted or metamorphosed. Their textures originated when the unit from which they were collected solidified. Their radiometric ages almost unambiguously date the magma's crystallization and, therefore, the unit's emplacement. No doubt remains that the sampled basalt flows originated as magmas melted within the Moon.

All nine sampling missions returned mare basalt, in greatly varying amounts. Apollos 11 and 12 landed on maria (table 1.2) and returned 16 and 36 rock-size (min 1 cm) basalt samples, respectively. The Apollo 11 material established the important fact that the maria are ancient in absolute age, though young stratigraphically. Subsequent studies showed that they were derived by partial melting from an already differentiated mantle source. Apollo 12 collected the youngest sample suite (see chap. 12) and proved that maria differ in age and composition from region to region. The remaining missions found a wide scatter in age and composition (see chap. 11), and partly clarified and partly complicated the picture of lunar-basalt petrogenesis. Apollos 15 and 17 were multipurpose missions that landed on mare surfaces and returned large amounts of basalt. Lunas 16 and 24 collected small cores of mare regolith. Even Apollos 14 and 16 and Luna 20, which landed on the terrae, obtained small bits of mare basalt. All the landing sites were near the margins of maria (pl. 4) or in the terrae (pl. 3). Therefore, only relatively thin basalt sections, and no central mascon sections, were sampled.

Composition

Lunar-mare rocks are designated "basalt" by the same general criteria used to define terrestrial basalt (Hubbard and Gast, 1971): They are dark-colored, mafic, fine-grained extrusive or shallow-intrusive rocks. Their textures are familiar from terrestrial basalt, except that they are fresher because they have not been chemically weathered (fig. 2.6). Clinopyroxene and plagioclase together compose 75 to 90 percent of most mare basalt; pyroxene is the more abundant mineral (Papike and others, 1976). Some compositional groups contain as much as 20 percent olivine and 24 percent optically opaque minerals (Fe-Ti oxides, of which ilmenite is the most abundant; Papike and others, 1976, table 3).

In elemental abundances, lunar-mare and terrestrial basalt differ substantially except in Ca content (10–11 weight percent CaO) (table 5.2; Hubbard and Gast, 1971; Taylor, 1975, 1982; Papike and others, 1976; Basaltic Volcanism Study Project, 1981, chap. 1). Lunar-mare basalt (1) contains no detectable H_2O; (2) is very low in alkalis (less than 1 weight percent), especially Na_2O; (3) is generally high in TiO_2—low lunar and average terrestrial contents are about the same; (4) is low in Al_2O_3 (8–15 weight percent) and SiO_2 (mostly 39–49 weight percent); maximum lunar and average terrestrial contents of these oxides are about the same; (5) is very high in FeO (17–22 weight percent)—higher than terrestrial basalt; and (6) is generally richer in MgO (7–18 weight percent)—the lowest lunar and average terrestrial contents are about the same. An additional important difference is in the extreme degree of reduction: Lunar-mare basalt contains essentially no Fe^{3+}; most Fe occurs as Fe^{2+}; and a minor amount of native Fe, formed by reduction at or near the surface, is always present (Basaltic Volcanism Study Project, 1981, chaps. 1, 3; Taylor, 1982, p. 292–294, 312).

Mare basalt also differs chemically from terra melt rocks of impact or volcanic origin. It is higher in FeO and MgO contents and lower in Al_2O_3 and CaO contents and Al_2O_3/CaO ratio. Its rare-earth-element patterns, as normalized to those of chondritic meteorites, generally have negative europium (Eu) anomalies, in contrast to the positive Eu anomalies of most terra materials (see chap. 8). Lunar basalt is very low in *siderophile elements*, elements that are concentrated in iron meteorites (see chap. 8). It differs further from impact melts in its lack of included debris. Lunar-mare basalt and terra materials—thus, the whole Moon—are very poor in volatiles (Wetherill, 1971; Taylor, 1975; 1982, p. 300–307).

Pyroclastic glasses, which constitute the dark-mantling materials, are partly similar and partly dissimilar to the mare lavas in bulk composition. Orange and black glasses from the Apollo 17 landing site are rich in Ti, but differ in trace elements and Mg from the high-Ti lavas in the same region (Heiken and others, 1974). Apollo 15 collected both Ti-poor green glasses and Ti-rich red glasses, neither of which are identical to the Ti-poor Apollo 15 lavas (Delano, 1979, 1980). Smaller amounts of other pyroclastic glasses are mixed in other sampled regoliths (Wood, 1975a).

Classification

Sampled mare basalt is generally classified on the basis of major-element content (table 5.2). Some authors distinguish sharply between high-Ti and low-Ti groups because the largest collections are very distinct in this element; Apollos 11 and 17 returned exceptionally Ti-rich basalt, whereas Apollos 12 and 15 returned low-Ti basalt (table 5.2; Papike and others, 1976; Taylor, 1975). The Ti gap is occupied by a few samples from the Apollo 12 landing site and small fragments from the Apollo 14 terra landing site (in breccia sample 14063, 7.3 weight percent TiO_2; Ridley, 1975). Small fragments of a very low titanium (VLT) group were found later in the Apollo 17 and Luna 24 regoliths (Papike and Vaniman, 1978). High-Al, feldspathic basalt is recognized as a distinct category, although it also was recovered in only small amounts (Ridley, 1975; Taylor, 1975, 1982; Taylor and Jakes, 1977); it characterizes collections from the eastern maria (see chap. 11) and premare basalt of the mare type (chap. 9). Small rare glass droplets and fragments found in all regoliths may represent additional magma types (Wood, 1975a; Binder and others, 1980). The continuum of spectral classes (Pieters, 1978) suggests that the gaps in Ti content and in other discriminative compositions are filled by unsampled basalt types (Papike and Vaniman, 1978). Only about a third of the observed number of spectral classes may have been sampled (Pieters, 1978).

There is now good agreement about which groups are significant, but less agreement about the classifying nomenclature. Most designations include the sampling mission. The scheme used here (table 5.2; Basaltic Volcanism Study Project, 1981, sec. 1.2.9; Taylor, 1982, p.

TABLE 5.2.—*Classification of mare-basalt samples used in this volume*

[After Basaltic Volcanism Study Project (1981, sec. 1.2.9.) and Taylor (1982, table 6.1). All values in weight percent]

Group	Distinguishing chemistry	Al_2O_3	TiO_2	K_2O	MgO
Apollo 11 high-K high Ti basalt---	High K, high Ti-----	8-10	9-14	>0.3	7-10
Apollo 11 low-K high-Ti basalt----	Low K, high Ti------			.03-.11	
Apollo 17 low-K high-Ti basalt----	------do----------				
Apollo 12 ilmenite basalt---------	Intermediate Ti-----		5-9		
Apollo 12 pigeonite basalt--------	Low Ti, high Si-----		1.5-5		
Apollo 15 pigeonite basalt--------	------do----------				
Apollo 12 olivine basalt----------	Low Ti, high Fe, Mg				10-18
Apollo 15 olivine basalt----------	------do----------				
Apollo 17 very low Ti basalt------	Very low Ti--------	10-15	<1.5	<0.04	10-11
Luna 24 very low Ti basalt--------	Very low Ti, high Al				
Apollo 12 feldspathic basalt------	High Al, low Ti-----		3-5	0.1-0.15	7-9
Luna 16 feldspathic basalt--------	------do----------				
Apollo 16 feldspathic basalt------	High Al, low to intermediate Ti.				

282–284) lists the main chemical properties that distinguish sampled groups. Most group names also include the name of a characteristic mineral observed optically (a *modal mineral*); other classifications refer to a mineral that would theoretically crystallize from a melt of the rock's composition (*norm*). For example, the terms "pigeonite (low-Ca clinopyroxene) basalt" (table 5.2), "Si-rich basalt," and "quartz-normative basalt" have all been applied to the same Apollo 12 or Apollo 15 samples. The Apollo 17 basalt suite is subdivided by trace-element contents (see chap. 11; Rhodes and others, 1976; Warner and others, 1979). Although textural terms are also used to designate some groups (chap. 11), classifications based on texture cut across those based on sampling site and chemistry (Warner, 1971). Textural variety within a basalt suite from a given site reflects differences in the crystallization and cooling histories of the lavas more than differences in composition (Lofgren and others, 1975). Some compositional differences within a given site have resulted from minor fractionation after emplacement, though fewer than in many terrestrial lavas (Taylor, 1982, p. 334).

ORIGIN AND EMPLACEMENT

The mare-basalt magmas originated by partial melting of ultramafic mantle material (mostly or entirely olivine and pyroxene) (Basaltic Volcanism Study Project, 1981, chaps. 1, 3, 4, 9). The Eu anomaly and other trace-element data demonstrate that the mantle does not consist of primitive, undifferentiated lunar material but segregated from the bulk Moon soon after it formed 4.55 aeons ago (see chap. 8; reviews by Taylor, 1975, 1982).

As discussed in chapters 12 and 13, known basalt flows were extruded until 3.5 aeons after the Moon formed. Thus, a substantial time gap separated the global differentiation that formed the mantle source from the partial melting that led to basalt extrusion. Because formation of mare basalt was a two-stage process, a source of heat in addition to that remaining from planetary accretion was apparently necessary to initiate the second-stage melting (Taylor, 1975, 1982). The amounts of radioactive K, Th, and U believed to have been present in the source regions were sufficient to generate enough heat to melt the very small observed amounts of basalt (Taylor, 1982, p. 310). These radioactive elements are most abundant in the Ti-rich basalt.

This partial melting is generally thought to have taken place between 60 and 500 km below the surface (Taylor and Jakeš, 1974; Green and others, 1975; Kesson and Lindsley, 1976; Delano, 1979, 1980; Taylor, 1982, p. 325). More precise estimates are controversial, especially concerning high-Ti basalt. Various schemes have associated basalt composition with source composition, but, again, the data are equivocal and the interpretations diverse. For example, high-Ti basalt may be derived from clinopyroxene-rich zones, VLT magmas from olivine-orthopyroxene zones, and high-Al basalt from clinopyroxene-plagioclase zones (see summary and references by Taylor, 1982, p. 330). The mantle may be crudely layered; one suggestion is that the low-Ti source lies 150 to 250 km below the surface, the high-Ti source 100 to 150 km deep, and the high-Al source 60 to 100 km deep, immediately beneath the crust (Taylor and Jakeš, 1974). Alternatively, the high-Ti source may be lower than the low-Ti source (Nyquist and others, 1977). Delano (1979, 1980) suggested that the pyroclastic glasses originated at the greatest depths, possibly 400 to 500 km below the surface, in an environment where carbon-oxygen gases may have formed (Sato, 1979).

The presence of glass and the vesicularity of many lavas are the only major indications of volatile activity on the Moon. The fact that their eruptions were driven by volatiles may explain why patches of dark-mantling materials appear where no lavas are known, as in such isolated craters as Petavius and Humboldt (fig. 4.2).

Whether or not layering exists in the mantle, the variety of sampled and unsampled compositions indicates considerable vertical and horizontal heterogeneity in the basalt-source zones. In particular, the compositional variety of basalt erupted at a given site simultaneously or within a very short time suggests that the sources were compositionally heterogeneous over short distances (see chaps. 11, 12; Green and others, 1975; Rhodes and others, 1976, 1977; Nyquist and others, 1979a; Taylor, 1982, p. 301, 320–321).

After the magmas were generated, most were modified in the original magma chambers, on the way to the surface, or on the surface (Basaltic Volcanism Study Project, 1981, p. 399–408, 498–513, 577–591). On the Moon as on the Earth (and probably all planets), early-formed crystals fractionated from the liquid magma, mantle or crustal materials were assimilated, and magmas from separate chambers mingled. Only a few magmas may have been primary in the sense that they remained unchanged after melting of the mantle source.

This volume can best contribute to the multifaceted question of mare-basalt origin by examining the geologic setting and emplacement histories of the observed mare units. Therefore, I consider why maria are concentrated in basins, especially in particular basins.

Basic hydrostatic principles suggest that extrusion of basaltic magmas is favored by (1) depressed surface elevations, (2) thin crusts and lithospheres, (3) low magma densities, and (4) deep melting sites (Solomon, 1975; Wilson and Head, 1981). Conditions 1 and 2 are most favorable in basins. A basin impact removes several kilometers or tens of kilometers of crustal material. The resulting depression is greatly reduced by an uplift of the mantle to compensate for the lost mass (chap. 4) but will partly survive if the lithosphere is strong. Addition of the ejecta also thickens the crust near the basin by a few kilometers. The depression not only collects whatever magmas are extruded but also contains most of the extrusion vents (fig. 5.24). Even if magmas melt at the same depth and ascend with equal freedom everywhere on the Moon, more would be extruded in the depressions than on the adjacent terra. A rising column of magma that would be erupted in a basin may only be intruded as dikes and sills outside the basin.

Basins may also affect extrusion in more active ways. A basin impact generates heat that may aid the melting and weaken the lithospheric barrier to magma ascent (Solomon and Head, 1980, p. 134). Subbasin structures, such as fractured or brecciated zones similar to those beneath craters, may facilitate magma movement and divert some magmas to extrusion sites high on the basin periphery (figs. 5.10*D*, 5.16; G, fig. 5.24).

Superposition of two or more basins or large craters enhances the likelihood of mare extrusion at a given spot. The first or the only extrusions will occur in the superposed excavations (Head, 1976a).

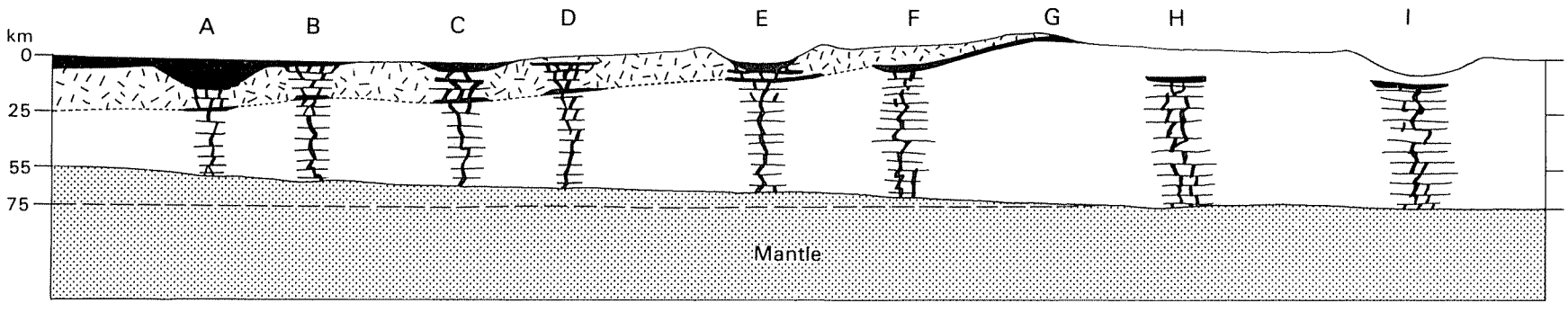

FIGURE 5.24.—Diagrammatic cross section of typical basin 1,000 km in diameter; no vertical exaggeration. Crust is about 75 km thick outside basin (see chap. 1) and is estimated at 55 km thick beneath basin center; deformed zone (above dotted line) is estimated at 25 km thick, and mantle uplift at 20 km. Magma-ascent paths, 60 km high above mantle surface, are indicated diagrammatically in nine places (A–I) as systems of dikes and sills. At A, lava was extruded onto floor of a crater superposed on the basin, and spilled beyond crater rim; at B, lava was extruded directly onto basin floor; extrusions A and B combined to flood basin center. At C, lava was extruded onto trough but did not overtop trough edges. At D, crust was too thick to allow an equal column of magma to be extruded. At E, floor of superposed crater decreased magma-ascent path by amount necessary to allow extrusion; crater interior was flooded. At F, contact of deformed zone and less severely deformed crust afforded path for lateral migration of lava, which was extruded high on basin flank at G. Crust at H and I outside basin was too thick to allow extrusion, even beneath a crater (I) equal in depth to the flooded craters inside basin.

This association is clearly illustrated on the farside, where such craters as Leibnitz, Lyot, and von Kármán and such small basins as Apollo, Planck, and Poincaré, all of which are superposed on the South Pole-Aitken and Australe basins, contain most of the farside's maria (pl. 4; fig. 5.25). In my opinion, similar superpositions of the still-larger Imbrium, Serenitatis, Tranquillitatis, Nubium, and other basins on the 3,200-km-diameter Procellarum basin cause the familiar concentrations of nearside maria.

Factors other than basin distribution have also been thought to affect mare distribution. Differential crustal thickness is commonly cited as the explanation of the 15-fold hemispheric dichotomy in mare distribution (pl. 4); the farside crust is thought to be thicker than the nearside crust (chap. 1). The Procellarum basin, however, may cause the difference. All the Moon's major maria except Crisium, Fecunditatis, Humboldtianum, Nectaris, Orientale, and Smythii lie in basins superposed on Procellarum (fig. 5.26). Of these maria, only Crisium contains a thick section of mare, and Mare Crisium is much smaller (500 km) than would be expected from the Moon's fourth largest basin (1,060 km diam; chap. 9; table 4.1).

The relative importance of magma density and melting depth is difficult to evaluate because of the many unknowns. High-Ti magmas are the densest, and high-Al magmas the least dense (Solomon, 1975). In the scheme of Taylor and Jakeš (1974), low-Ti magmas originate at greatest, and high-Al magmas at shallowest, depths. Thus, density and depth may cancel each other as factors favoring extrusion. Basin-controlled crustal thickness may play a greater role in affecting the composition of extruded lavas. High-Al magmas preferentially fill basins formed in thick crusts (Fecunditatis, Nectaris, Smythii), whereas low-Ti magmas preferentially form over thin crusts (in the Procellarum basin, especially where Serenitatis and Imbrium are superposed on that giant basin). These factors are further evaluated in chapters 11 and 12 after the historical dimension has been added.

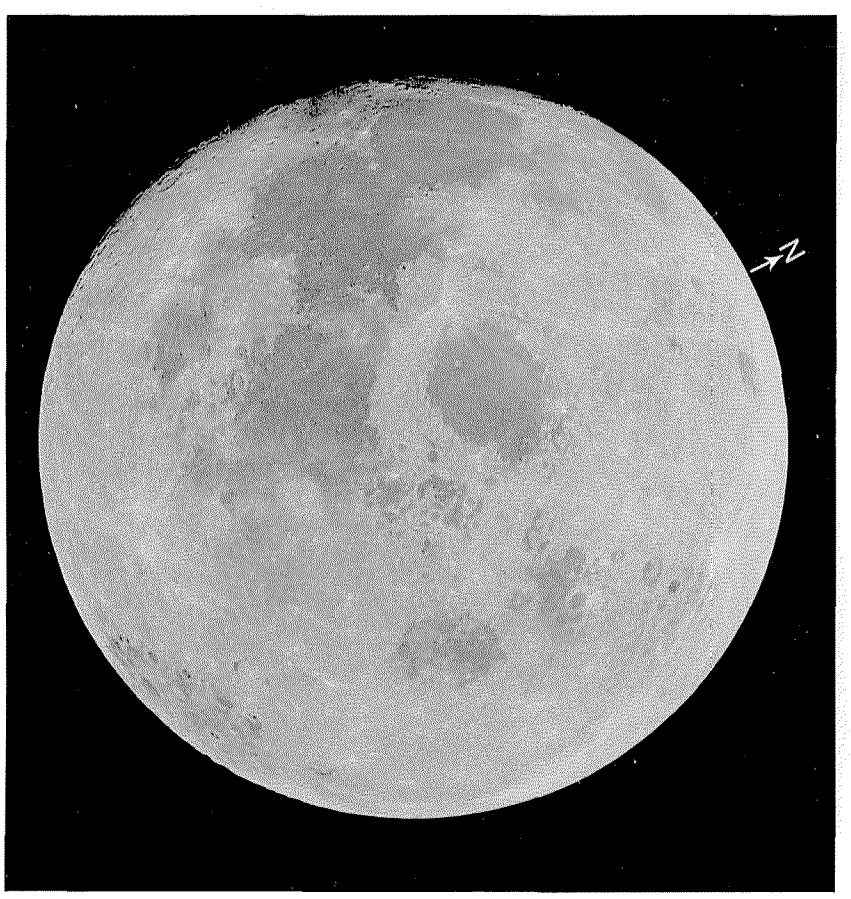

FIGURE 5.25.—Eastern nearside, east limb, and part of farside of Moon, showing spotty distribution of mare patches in sparsely flooded Australe basin (lower right edge), peripheral "lakes" concentric with Crisium basin, and other maria outside main mare concentration. Apollo 11 frame H–6665, taken during return to Earth after first lunar landing.

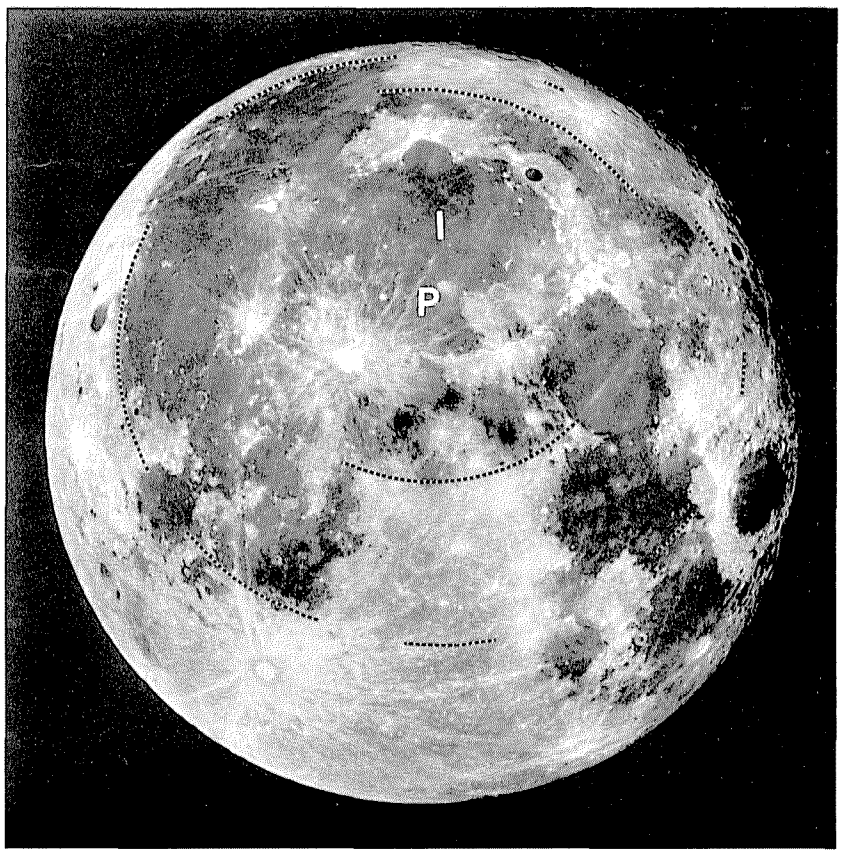

A

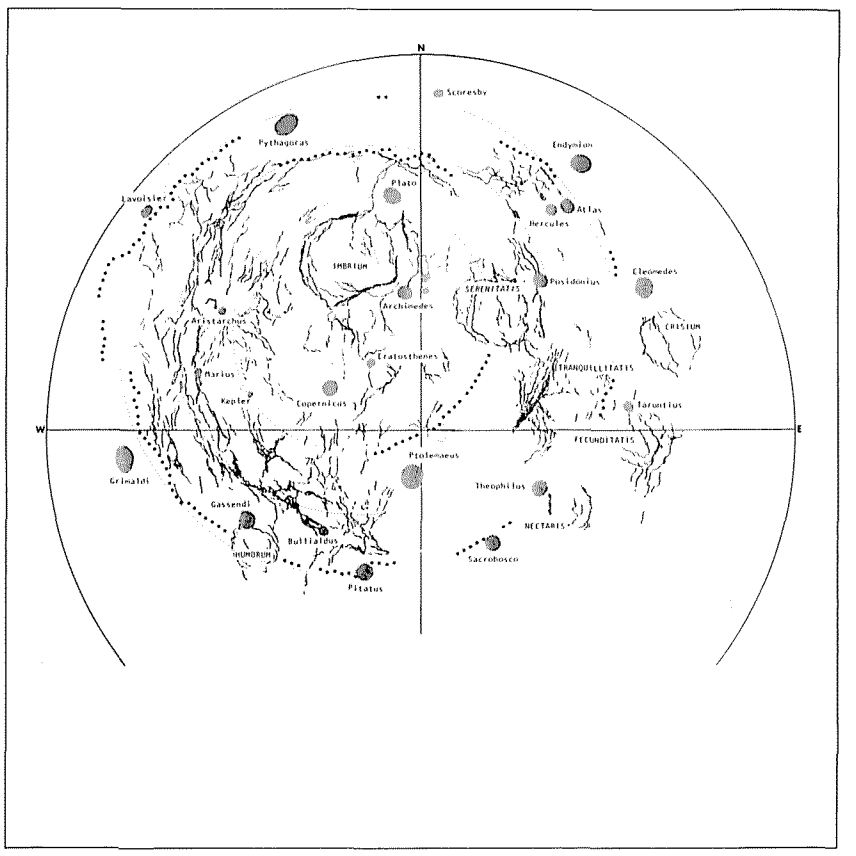

B

FIGURE 5.26.—Procellarum basin as drawn by Whitaker (1981). Courtesy of E.A. Whitaker.

A. Telescopic full-Moon photograph of nearside, showing center (P) and parts of three rings of Procellarum basin. I, center of Imbrium basin. Maria are concentrated inside largest ring of Procellarum basin. In much early work, an asymmetry in basin distribution was thought to cause the hemispheric dichotomy in mare distribution, but basins are distributed randomly (pl. 3); Procellarum may account for most of the dichotomy. Right side of photograph overlaps with left side of figure 5.25. From Whitaker (1981, fig. 2).

B. Observed scarps and terra margins concentric with basin (large dots), complete rings that best fit the topography (small dots), mare ridges (lines; see chap. 6), and major landmarks. From Whitaker (1981, fig. 1).